HHS Public Access

Author manuscript

J Immunol. Author manuscript; available in PMC 2018 March 15.

Published in final edited form as:

J Immunol. 2017 March 15; 198(6): 2269–2285. doi:10.4049/jimmunol.1600610.

Loss of Twist1 in the Mesenchymal Compartment Promotes Increased Fibrosis in Experimental Lung Injury By Enhanced Expression of C-X-C Motif Ligand 12 (CXCL12)

Jiangning Tan[1], **John R Tedrow**[1], **Mehdi Nouraie**[1], **Justin A Dutta**[1], **David T Miller**[1], **Xiaoyun Li**[1], **Shibing Yu**[1], **Yanxia Chu**[1], **Brenda Juan-Guardela**[2], **Naftali Kaminski**[2], **Kritika Ramani**[3], **Partha S Biswas**[3], **Yingze Zhang**[1], and **Daniel J Kass**[1]

[1]Dorothy P. and Richard P. Simmons Center for Interstitial Lung Disease and the Division of Pulmonary, Allergy, and Critical Care Medicine, University of Pittsburgh, Pittsburgh, PA

[2]Section of Pulmonary, Critical Care, and Sleep Medicine, Yale University, New Haven, CT

[3]Division of Rheumatology, University of Pittsburgh, Pittsburgh, PA

Abstract

Idiopathic Pulmonary Fibrosis (IPF) is a disease characterized by the accumulation of apoptosis-resistant fibroblasts in the lung. We have previously shown that high expression of the transcription factor twist1 may explain this pro-survival phenotype *in vitro*. However, this observation has never been tested *in vivo*. We found that loss of twist1 in COL1A2+ cells led to increased fibrosis characterized by very significant accumulation of T-cells and bone marrow-derived matrix-producing cells. We found that twist1-null cells expressed high levels of the T-cell chemoattractant CXCL12. *In vitro*, we found that the loss of twist1 in IPF lung fibroblasts increased expression of CXCL12 downstream of increased expression of the non-canonical NF-κB transcription factor RelB. Finally, blockade of CXCL12 with AMD3100 attenuated the exaggerated fibrosis observed in twist1 null mice. Transcriptomic analysis of 134 IPF patients revealed that low expression of twist1 was characterized by enrichment of T-cell pathways. In conclusion, loss of twist1 in collagen-producing cells led to increased bleomycin-induced pulmonary fibrosis, which is mediated by increased expression of CXCL12. Twist1 expression is associated with dysregulation of T-cells in IPF patients. Twist1 may shape the IPF phenotype and regulate inflammation in fibrotic lung injury.

Introduction

One theory of the pathogenesis of Idiopathic pulmonary fibrosis (IPF) suggests that a fibroblast of a very distinct phenotype, following an unknown injury, accumulates in the

AUTHOR CONTRIBUTIONS

Experiments were performed by JT, JAD, YC, BJG, DTM, SY, XL,YC, and KR. Experiments were designed and data were analyzed by JT, JRT, MN, NK, PSB, YZ, and DJK. The manuscript was written by JT, JRT, YZ, and DJK.

Ethical Statement

This work was approved by the Institutional Review Board and the Institutional Animal Care and Use Committee of the University of Pittsburgh.

lung—a fibroblast that "paradoxically" demonstrates little apoptosis (1) despite a microenvironment in the lung that is hostile to cell survival (2, 3). Evidence for this theory comes from e*x vivo* fibroblasts derived from IPF lungs that demonstrate resistance to pro-apoptotic stimuli compared to normal human fibroblasts (4). Recent data suggest that signals derived from the extracellular matrix (5) drive the so-called "IPF phenotype." Persistence of fibroblasts in fibrotic lungs may be due to soluble survival factors (6) or may result from cell-autonomous pro-survival signaling, possibly through Akt-related pathways (7, 8). We have previously shown that the transcription factor twist1 is one of the most highly expressed transcription factors by gene expression profiling of IPF lungs and may mediate the pathologic pro-survival phenotype of fibroblasts *in vitro* (3). However, *in vivo* data demonstrating the relevance of twist1 to human or experimental pulmonary fibrosis have been lacking.

Twist1 is a member of the basic helix-loop-helix family of transcription factors and is critical for mesoderm differentiation in Drosophila (9). Twist1 mutations in humans leads to Saethre-Chotzen syndrome (10), and twist1 knockout mice die *in utero* due to incomplete neural tube closure (11). Twist1 has multiple functions that may be relevant to the pathogenesis of pulmonary fibrosis including inhibition of NF-κB inflammatory cells (12, 13). In cancer, twist1 expression is a potent pro-survival factor portending a poor prognosis (14) and contributes to the resistance of cancers to chemotherapy-induced apoptosis (14). Related to the cancer phenotype, and perhaps most relevant to fibrosis is the role of twist1 in epithelial-mesenchymal transition (EMT) (15, 16), a process which has been suggested as a source of matrix-producing cells in fibrosis. We hypothesized that a strategy to silence expression of twist1 in fibroblasts would block fibrosis by counteracting the pro-survival phenotype and thus promote a fibroblast that is susceptible to apoptosis. For this study, we tested the hypothesis that transgenic mice with loss of twist1 in the mesenchymal compartment would be protected from experimental lung fibrosis. These animals, in the presence of tamoxifen, are engineered to express cre recombinase in collagen-expressing cells (COL1A2) (17) and to excise the twist1 locus flanked by loxP sites (twist1 FL) (18).

Materials and Methods

Reagents

Monoclonal antibody against Twist (clone 2C1a) was purchased from Abcam (Cambridge, MA). Antibodies to RelB (clone C1E4), and RelA (clone C22B4) were from Cell Signaling Technology (Danvers, MA). Anti-CXCL12 (clone K15C) was from EMD Millipore (Billerica, MA). Collagen type I and CXCR4 (immunoblotting) antibodies were obtained from Rockland (Limerick, PA). An antibody against β-actin was purchased from Santa Cruz Biotechnology (Dallas, TX). Quantikine ELISA kit for Mouse CXCL12/SDF-1α was from R&D Systems (Minneapolis, MN). All secondary antibodies were from Jackson ImmunoResearch (West Grove, PA). Bleomycin, tamoxifen, AMD3100, collagenase type I, Deoxyribonuclease I (DNase I), Brefeldin A, sodium orthovanadate, and a monoclonal antibody against α-smooth muscle actin (clone 1A4) were purchased from Sigma-Aldrich (St. Louis, MO). Wortmannin was obtained from Enzo (Farmingdale, NY). Sircol collagen assay kit was purchased from Biocolor (Belfast, UK). Short interfering RNA

oligonucleotides (siRNA) and non-targeting controls (SMARTPOOL) were purchased from Dharmacon (Lafayette, CO). HiPerFect Transfection Reagent, RNeasy Plus Mini Kit and all primers for RT-PCR were from Qiagen. RT-PCR primers specific for mouse Twist1, Collagen1, Fibronectin1 (Fn1), Acta2, MIF, CXCL9, CXCL10, CXCL11, CXCL12, CCL19, and CCL21; human twist1, CXCL12, and RelB and the endogenous mouse/human housekeeping gene PPIA were obtained from Qiagen (Valencia, CA). Chemiluminescence Plus Kit was purchased from Perkin-Elmer (Boston, MA). Power SYBR Green and High-Capacity cDNA Reverse Transcription Kit were from Applied Biosystems (Foster City, CA).

Isolation of human lung tissue

Human lung tissues were obtained from excess pathologic tissue after lung transplantation and organ donation, under a protocol approved at the University of Pittsburgh Institutional Review Board (19). IPF tissues were obtained from explanted lungs of subjects with advanced disease and normal lungs were donated organs not suitable for transplantation from the Center for Organ Recovery and Education (CORE). Lung tissues were stored at −80°C.

Primary Human Lung Fibroblast Culture

Human primary lung fibroblasts were cultured from the explanted normal lungs from organ donors or from the lungs of patients with IPF undergoing lung transplant surgery as previously described (20). All primary lung fibroblasts were maintained in DMEM supplemented with 10% Fetal Bovine Serum (FBS) and 1% antibiotic-antimycotic and were used between passages 3 to 6.

Twist1 conditional knockout mice

ROSA26-STOP tdTomato+ mice were purchased from Jackson (Bar Harbor, ME). Mice expressing cre recombinase in collagen-expressing cells (COL1A2) in the presence of tamoxifen were generously provided by Dr Benoit DeCrombrugghe (MD Anderson Cancer Center) (17). Mice expressing twist1 flanked by loxP sites (twist1 FL) were generously provided by Dr Gerard Karsenty (Columbia University) (18). The three strains were bred to generate triple transgenic mice. Control mice expressed cre and tdTomato with two wildtype twist1 alleles. All mice were subjected to intraperitoneal (IP) injection of tamoxifen (80mg/kg for 5 days) at 5 weeks and 6 additional injections delivered three times per week beginning at 8 weeks of age during bleomycin injury experiments.

Bleomycin-Induced Lung Injury and treatment with AMD3100

8-week-old mice were anesthetized with isoflurane in an anesthesia chamber. Bleomycin was administered at 2U/kg by inhalation (21). Beginning from day 1 after bleomycin injury, the antagonist of the CXCL12 receptor CXCR4, AMD3100, or the vehicle (sterile water) was subcutaneously injected at 5 mg/kg daily (22). Mice were sacrificed on day 14.

Immunofluorescence

Immunofluorescent staining of mouse lungs was performed as previously described (21). Briefly, mouse lungs were inflated to 25 cm H_2O pressure with 4% paraformaldehyde

(PFA), and the tissue was excised and submerged in PFA for one hour. The tissue was then cryoprotected overnight in 30% sucrose. Five μm sections were cut and mounted. Tissue was then re-fixed and permeabilized with 0.2% triton-X. Tissue was stained for α-smooth muscle actin and surfactant protein C (Seven Hills Bioreagents, Cincinnati, OH) and CD45 (Ebioscience, San Diego, CA). Cy5-conjugated secondary antibodies were from Jackson Immunoresearch. Tissue was mounted with DAPI and anti-fade.

Sircol Assay for Acid-Soluble Collagen

Mouse lungs were perfused through the right ventricle with PBS. The left lungs were excised and flash-frozen in liquid nitrogen, followed by lyophilization in preparation for collagen determination by the Sircol collagen assay. Lungs were homogenized in 0.5M acetic acid with protease inhibitors (Sigma-Aldrich). The homogenate was pelleted, and the supernatant was run across a QIAshredder column (Qiagen). The lung-acetic acid mixture was incubated with the Sircol Red reagent. The collagen-dye complex was pelleted, and the precipitated material was re-dissolved in NaOH. Optical density at 540 nm (OD_{540}) was recorded using a microplate reader.

Single Cell Suspensions of Mouse Lungs for Flow Cytometry

Mouse lungs were minced into 1–2 mm pieces with sterile scissors and then incubated with 100mg/ml of collagenase I and 1mg/ml of DNase I in wash media (DMEM+5%FBS) at 37ºC. Cells were dispersed by gentle pipetting and filtered through a cell strainer to eliminate debris. Cells were pelleted and re-suspended in appropriate volume of Flow Cytometry Staining Buffer to achieve a final cell concentration of 2×10^7/ml. Sorting was performed in BD FACSAria II (BD Biosciences). Cells were stained with anti-CD45-FITC antibody (BioLegend; clone 30-F11). TdTomato samples were read in the PE channel with a 550LP Mirror and 585/42 Filter Set.

RNA Extraction, Nanostring analysis, and cDNA synthesis for RT-PCR of tdTomato+ cells isolated with Flow Sorting

Total RNA was extracted from tdTomato+ cells isolated from single cell suspensions of mouse lungs with flow sorting according to RNeasy Plus Mini Kit handbook. In one experiment, RNA was isolated and subjected to the Nanostring nCounter CodeSet for mouse inflammation. Complementary DNA (cDNA) was synthesized from the purified mRNA with the High-Capacity cDNA Reverse Transcription Kit according to manufacturer’s protocol (Applied Biosystems, Foster City, CA).

Quantitative RT-PCR

Quantitative RT-PCR amplifications were performed with the PowerSYBR Green PCR Master Mix and the ABI Prism 7900HT Fast Real-Time PCR System (Applied Biosystems, Foster City, CA).

Bronchoalveolar Lavage (BAL) and Detection of CXCL12 by Enzyme-Linked Immunosorbent Assay (ELISA)

Immediately after euthanasia, mice were subjected to median sternotomy, and the trachea was exposed and intubated with an 18G catheter. 1 ml of sterile saline was instilled into the lung through the tracheal catheter at a pressure of 20 cm water, and cells were retrieved. Cells in the BAL fluid were isolated by centrifugation. The supernatant was collected and processed to detect CXCL12 by the Quantikine ELISA kit according to the manufacturer's instructions. Active TGFβ from BAL was measured using an ELISA kit from BioLegend (San Diego, CA). Additional cytokines were analyzed using the Luminex mouse 23-plex cytokine kit and a Bio-Plex 100 according to the manufacturer's instructions (Bio-Rad Systems, Austin, TX).

Flow Cytometry

BAL cells were counted by trypan-blue exclusion method followed by incubation with CD16/CD32 antibody (BD Pharmingen) for 30 min on ice. Mouse bone marrow cells were obtained as previously described (23). Cells were then stained with the following: Ly6G-FITC (BD Pharmingen; clone IA8), CD68-PE (Bio Legend; clone FA-11), CD3-APC (BD Pharmingen; clone 145–2011), B220-PeCy7 (BD Pharmingen; clone RA3–6B2), CD4-V450 (BioLegend; clone RM4–5), CD8-PerCP (BD Pharmingen; clone 53-6.7) and Rat Anti-Mouse CD184/CXCR4 (BD Pharmingen; clone 2B11. FITC-Anti-Mouse/Rat Ki67 and Rat IgG2a κ Isotype Control was from Ebioscience (San Diego, California). Samples were acquired on a FACSAria II or Fortessa (BD Biosciences, San Jose CA) and analyzed by FlowJo software (Tree Star, Ashland OR). Intracellular cytokine staining of cells obtained from single cell suspensions of mouse lungs was performed as described previously(24). Briefly, cells were *ex vivo* stimulated with PMA and ionomycin (Calbiochem, La Jolla, CA, USA) in the presence of Monensin (BD Pharmingen, San Diego, CA, USA) for 4–6 h. Cells were stained for intracellular IFN-γ, IL-4, and IL-17A with anti-IFNγ (BD Pharmingen; clone XMG1.2), anti-IL-4 (BD Pharmingen; clone 11B11) and anti-IL-17 (Ebioscience; clone eBio1787) antibodies. Intracellular staining was performed using the BD intracellular cytokine staining kit (BD Pharmingen), followed by flow cytometry. Staining of Foxp3 was performed with the mouse Foxp3 staining kit (EBioscience, San Diego, CA, USA).

Gene Silencing in human lung fibroblasts

Complexes with short-interfering RNA oligonucleotides (siRNA) or scrambled controls were transfected employing the HiPerfect Transfection Reagent according to the manufacturer's recommendations (Dharmacon). Twist1 or control siRNA complexes were transfected on the day of plating (Day 0) and the next day (Day 1). Silencing of additional targets was performed consecutively on Days 1 and 2.

Immunoblotting

After incubation with twist1/control siRNA, IPF lung fibroblasts were lysed for immunoblotting to measure the protein expression of Twist1, CXCL12, Collagen I, α-SMA, β-actin, RelA, and RelB. Immunoblotting was performed as previously described (25). Cells were treated with brefeldin A at one hour prior to lysis to inhibit secretion of CXCL12.

Identification of E-Box binding motifs in CXCL12 and RelB gene and Chromatin Immunoprecipitation Assays (ChIP)

E-Box binding motifs, CANNTG, were identified by simple sequence scanning for the 5′UTR and an additional 2 kb upstream sequences of both gene using Sequencher 5.0 (Genecode) for human CXCL12 and RelB. The identified E-Box binding motifs were further characterized using chromatin immunoprecipitation (ChIP) assays. The ChIP assay was performed as described (26, 27). Chromatin was precipitated with antibodies against twist1, mouse IgG1, or rabbit IgG as controls. DNA from the pull-down reactions and the input DNA were used as template for PCR employing primers designed to amplify the regions containing putative E-box binding motifs. A total of 5 and 12 potential E-box binding sites were identified in CXCL12 and RelB promoter respectively. An antibody specific for Pol II DNA polymerase was used as a positive control. Due to the proximity of these binding sites, primers were designed to test multiple sites as a single unit for some of these E-box binding motifs. The locations of the putative E-box binding motifs and the primers used for the PCR amplification specifically for each site are listed in Table 1. The PCR products were analyzed using agarose electrophoresis.

Microarray Analysis

The RNA isolation and microarray procedures have been previously described(28, 29). These data are publically available from the Lung Genomics Research Consortium (LGRC) website (http://www.lung-genomics.org/). 134 IPF patients and 108 normal controls were selected. Table 2 describes the LGRC cohort. These data and methods are available on the Gene Expression Omnibus Database (GEO) under reference number GSE47460. The data were normalized using a cyclic loess algorithm from the Bioconductor suite of R tools (30). Analyses were performed using BRB-ArrayTools 4.3.0 Stable Release developed by Dr Richard Simon and the BRB-ArrayTools Development Team. Additional gene expression data were obtained from GEO (GSE10667, https://www.ncbi.nlm.nih.gov/geo/) (31).

Statistical Analysis

Data in these studies were analyzed by t-test, ANOVA followed by Fisher’s LSD or the Neuman-Keuls post-hoc tests, or chi-square testing using Prism 6.0 (GraphPad).

RESULTS

Loss of twist1 in COL1A2+ cells leads to increased bleomycin-induced pulmonary fibrosis

Based on our previous data showing that loss of twist1 leads to apoptosis in lung fibroblasts(3), we hypothesized that loss of twist1 in experimental pulmonary fibrosis would be characterized by enhanced fibroblast apoptosis and protection from pulmonary fibrosis. To test this hypothesis, we bred mice expressing tamoxifen-inducible cre recombinase in collagen-expressing (COL1A2+) cells (17) and twist1 flanked by loxP sites (twist1 FL) (18) or wild type controls (twist1 WT). In addition, we bred the ROSA-26 tdTomato reporter (32) to identify the cells undergoing cre-mediated recombination. The strategy is shown in Figure 1A–C. Following injury with bleomycin, immunofluorescent staining showed tdTomato expression in cells limited to the mesenchymal compartment (Figure 1D) including cells that

morphologically appeared to be fibroblasts as well as airway and vascular smooth muscle cells. Endothelial cells did not demonstrate tdTomato expression. Alpha-smooth muscle actin staining was essentially limited to airway and vascular smooth muscle cells. No tdTomato+ cells co-expressed the type 2 alveolar epithelial cell marker, surfactant protein C (SFTPC) (Figure 1D). Cells co-expressing the common leukocyte antigen CD45 (33, 34) and tdTomato were also identified *in situ* (Figure 1E). Expression of tdTomato was then used by flow cytometry to isolate all the cells in the lung that have undergone cre-mediated recombination. Following administration of tamoxifen, cells were flow-sorted from twist1 WT and twist1 FL mice and processed for quantitative RT-PCR (Figure 1F). Cells from twist1 FL mice expressed significantly less twist1 at the mRNA level. At 14d following administration of saline by inhalation as a control for bleomycin injury, no differences were observed between twist1 WT and twist1 FL animals (Figure 1G). Following injury with bleomycin, much to our surprise, the histology in the twist1 FL animals, as compared to twist1 WT controls, was characterized by more confluent areas of injury and matrix deposition as well as lymphoid aggregates. To quantify both injury and fibrosis, we performed the following analyses: first, we quantified acid-soluble collagen as we have done previously (Figure 1H)(25). No difference was observed between uninjured WT and FL animals. In contrast, significantly more collagen was detected in twist1 FL animals compared to twist1 WT animals suggesting that, in fact, loss of twist1 in COL1A2+ cells was associated with more severe injury and fibrosis. Next, we analyzed the flow-sorted cells as described above for expression of several fibrotic markers by quantitative RT-PCR: COL1A1, fibronectin (Fn1), and α-smooth muscle actin (Acta2) (Figure 1I–K). Significantly increased expression of all three genes was observed in the twist1 FL animals further supporting the observation of increased bleomycin-induced pulmonary fibrosis in these animals. Finally, we quantified the total number of tdTomato+ cells as a marker of COL1A2+ cell accumulation in the lung (Figure 1L–M). After digestion of and dispersion of lungs from bleomycin-injured twist1 WT and twist1 FL animals into single cell suspensions, we found significantly more tdTomato+ cells from the twist1 FL animals compared to the WT controls. To determine if this population of tdTomato+ cells arose from a local population or from a bone marrow-derived population, we also quantified the number of tdTomato+CD45+ cells (Figure 1L–O). No significant difference was observed between CD45−/tdTomato+ cells. However, CD45+tdTomato+ cells were more frequently observed in twist1 FL animals. These data suggest that loss of twist1 in COL1A2+ cells led to increased bleomycin-induced pulmonary fibrosis by several mechanisms including the accumulation of a bone marrow-derived matrix-producing population of cells and increased matrix synthetic activity in these cells.

Loss of twist1 in COL1A2+ cells was associated with the increased accumulation of T-cells in the lung

Histologically, the twist1 FL mice injured with bleomycin appeared to have a more extensive inflammatory infiltrate (Figure 1). To further characterize the inflammatory infiltrate of bleomycin and uninjured controls, we analyzed the cells recovered from bronchoalveolar lavage (BAL) by flow cytometry (Figure 2). BAL cells were stained for Ly6G to mark neutrophils, CD68 to mark macrophages, CD3 to mark T-cells, and B220 to mark B-cells. While not statistically significant, twist1 FL mice were characterized by a trend towards

more neutrophils between the uninjured and the bleomycin-injured mice (Figure 2A, B). This is consistent with increased injury in the twist1 FL mice. Uninjured twist1 FL mice had significantly fewer CD68+ cells compared to WT. There was a significant accumulation of CD68+ cells in twist1 FL mice after bleomycin injury compared to the uninjured (Figure 2A, C). Following bleomycin injury, the most significant observation was the large accumulation of CD3+ cells in bleomycin-injured twist1 FL mice compared to bleomycin-injured twist1 WT controls (Figure 2A, D). While it did not reach statistical significance, more CD3+ cells were observed in twist1 FL mice in the absence of injury compared to twist1 WT mice. There were significantly fewer B220+ cells in uninjured twist1 FL mice compared to uninjured WT controls, but the same difference was not observed following bleomycin injury (Figure 2A, E). These data show significant shifts in the inflammatory infiltrate between twist1 WT and FL animals.

To further subphenotype the infiltrating T-cells based on their functionality, we generated single cell suspensions of bleomycin-injured lungs from twist1 WT and FL mice, and the cells were stimulated for intracellular cytokine staining (Figure 3). Consistent with previous results, the average number of cells isolated from the single cell suspension of bleomycin-injured twist1 FL mice was higher than the WT controls (*data not shown*). This result largely drives the differences between the genotypes for absolute counts of cells. There was no significant difference in terms of the percentage of CD4+ cells. However, more CD4+ cells were stained from the bleomycin-injured twist1 FL mice (Figure 3A,D). Of the cells isolated, more cells in the twist1 FL mice were CD4+IFNγ+ (Figure 3A,E), indicating a Th1 phenotype of T-helper cells population. However, no significant differences were observed between genotypes for CD4+IL4+ (Th2) or CD4+IL17+ cells (Th17) (Figure 3A,F,G). The percentage of CD4+Foxp3+ cells did not differ between genotypes (Figure 3B,H). However, there were absolutely more CD4+FoxP3+ cells in the twist1 FL mice compared to WT controls. By absolute numbers, CD4+Foxp3+ cells appeared to be the most enriched subphenotype of T-cell isolated. As with CD4, there was no significant difference between the percentage of CD8+ cells between genotypes, but more CD8+ cells were detected in the twist1 FL mice (Figure 3C,I). For all subphenotypes of CD8+ cells, more IFNγ+, IL4+, and IL17+ cells were present in the twist1 FL mice compared to WT controls (Figure 3C,J–L). Overall, these data show that the loss of twist1 FL mice in COL1A2+ cells leads to derangements in the inflammatory infiltrate including increased accumulation of CD68+ and CD3+ cells in bleomycin-injured lungs. The T cells, which include both T-helper cells (CD4+ T cells) as well as cytotoxic T cells (CD8+) that express IFNg, IL-4 and IL-17, likely contribute to the enhanced tissue injury in twist1 FL mice.

Loss of twist1 in COL1A2+ cells is associated with increased expression of the T-cell chemoattractant chemokine (C-X-C motif) Ligand 12 (CXCL12)

If T-cells and tdTomato+ cells accumulate in bleomycin-injured lungs following loss of twist1 in COL1A2+ cells, we reasoned that COL1A2+ twist1 null cells must secrete a soluble signal to call these cells into the lung. To investigate potential soluble signals that might be secreted by twist1 null cells, we analyzed the bronchoalveolar lavage (BAL) for multiple cytokines and chemokines by the Luminex platform (Figure S1). Consistent with the derangement of T-cells reported in Figure 3, we found multiple inflammatory mediators

expressed at higher levels in twist1 null mice. To determine if any of these factors are expressed in COL1A2+Cre-ER(T) twist1 FL cells, we subjected the RNA from the flow-sorted cells to the Nanostring platform (Table S1). We found no concordant results between the Luminex and the Nanostring data. We also performed an ELISA for active TGFβ and found no differences between bleomycin-injured twist1 WT and twist1 FL animals (Figure S1O). One potentially important chemokine candidate that we considered is (C-X-C Motif) Ligand 12 (CXCL12). CXCL12 is a potent chemoattractant (33) for T-cells and so-called "fibrocytes." First, we analyzed the concentration of CXCL12 in the BAL ELISA (Figure 4A). We found significantly more CXCL12 in the BAL of twist1 FL mice compared to twist1 WT controls following bleomycin injury. To confirm that the increase in CXCL12 may be in part due to increased expression in tdTomato+twist1 FL cells, we analyzed CXCL12 by quantitative RT-PCR from the flow-sorted cells (Figure 4B). We found a nearly fourfold increase in CXCL12 mRNA in tdTomato+twist1 FL cells compared to tdTomato +twist1 WT controls. We also tested other chemokine candidates with T-cell chemoattractant activity including CXCL9, CXCL10, CXCL11, CCL19, and CCL21. But we found no differences between twist1 FL and WT mice (*data not shown*). To explore a possible link between twist1 and CXCL12, we then moved to human fibroblasts isolated from normal and IPF lungs. In these experiments, we determined if silencing of twist1 expression by short-interfering RNA (siRNA) was associated with increased expression of CXCL12. In lung fibroblasts from normal lungs, silencing of twist1 led to a significant reduction in twist1 mRNA (Figure 4C). However, a small but significant increase in CXCL12 mRNA was observed (Figure 4D). In IPF lung fibroblasts, however, silencing of twist1 by siRNA was associated with a fourfold increase in CXCL12 mRNA (Figure 4E). We repeated these experiments and processed the cells for immunoblotting for twist1 and CXCL12 in addition to the fibrosis markers collagen I and α-smooth muscle actin (Figure 4F–J). Silencing of twist1 protein was more pronounced in IPF fibroblasts as shown in the representative immunoblot and by quantitative densitometry (Figure 4F,G). Loss of twist1 was associated with increased CXCL12 in normal lung fibroblasts and to an even greater extent in IPF lung fibroblasts (Figure 4F,H). Loss of twist1 in normal lung fibroblasts led to a very significant increase in expression of collagen I. This increase was much less pronounced in IPF lung fibroblasts (Figure 4F,I). Loss of twist1 in normal lung fibroblasts was associated, possibly, with a small increase in expression of α-SMA. However, no difference in α-SMA expression was observed in IPF lung fibroblasts (Figure 4F,J). Hypoxia is a known and potent inducer of CXCL12 expression(35, 36). We silenced twist1 expression in IPF fibroblasts in the presence or absence of hypoxia (Figure 4K–M). Silencing of twist1 led to a significant increase in CXCL12 mRNA in the presence of normoxia by qPCR, and this difference was exaggerated in the presence of 5% O_2 atmosphere. We observed a nearly 25-fold increase in CXCL12 mRNA. However, by immunoblotting, no difference was observed in intracellular CXCL12. Taken together, these data indicate that in both COL1A2+ mouse cells and human lung fibroblasts, loss of twist1 is associated with increased expression of CXCL12.

Expression of CXCL12 mediated by the loss of twist1 is associated with events that occur downstream of activation of the non-canonical NF-κB complex by IKKα

CXCL12 has been shown to be regulated preferentially in response to non-canonical NF-κB signaling (p52/RelB) (37). Signaling specific for NF-κB2 activates several upstream kinases that phosphorylate IKKα homodimers, leading to phosphorylation of the transcriptionally-inactive NF-κB2/p100/RelB complex and proteasomal processing to the transcriptionally-active NF-κB2/p52/RelB heterodimer (38), nuclear translocation, and transcription of downstream targets including CXCL12 (37). We have shown that loss of twist1 is associated with increased expression of CXCL12 at the level of both mRNA and protein. But how loss of twist1 regulates CXCL12 is unknown. In this experiment, we sought to understand the effect of twist1 silencing on activation of IKKα and one of its upstream kinases MEKK1 (Map3k1) (39). Silencing of twist1 in IPF fibroblasts did not affect IKKα protein levels (Figure 5A). Simultaneous silencing of twist1 and IKKα completely blocked CXCL12 expression (Figure 5A–C) indicating that IKKα is central to the expression of CXCL12. IKKα expression appears to be independent of twist1. Twist1 silencing did not affect Map3k1 protein expression (Figure 5D–E). Silencing of twist1 alone had no effect on IKKα phosphorylation (Figure 5D,F). Silencing of Map3k1 does partially block phosphorylation of IKKα without an effect on total IKKα (Figure 5G). Silencing of Map3k1 completely blocks expression of CXCL12 while simultaneous silencing of twist1 partially overcomes this inhibition (Figure 5H). These data indicate that Map3k1 is a principal kinase regulating IKKα phosphorylation in IPF fibroblasts. Following silencing of Map3k1, IKKα remains phosphorylated and appears to be adequate for expression of CXCL12 following the silencing of twist1. Taken together, these data suggest that the actions of twist1 are distal to IKKα and may be related to the function of twist1 as a transcription factor.

Loss of twist1 is associated with increased expression of the non-canonical NF-κB transcription factor RelB

In these next experiments we focused on the role of twist1 as a transcription factor assaying targets downstream of IKKα (Figure 6). First, we determined the effect of twist1 on the non-canonical NF-κB family member RelB. Silencing of twist1 in IPF lung fibroblasts led to a nearly threefold increase in RelB mRNA (Figure 6A). Similarly, at the level of protein there was a dramatic increase in RelB protein upon silencing of twist1 (Figure 6B–D). Silencing of RelB in the presence or absence of twist1 expression completely blocks both RelB expression and CXCL12 (Figure 6B,D). This effect led us to suspect that twist1 may affect expression of RelA, a principal canonical NF-κB transcription factor regulating RelB expression in immune cells(40). Silencing of twist1 had no effect on RelA expression (Figure 6E–G). Simultaneous silencing of RelA completely blocked RelA while expression of RelB actually *increased* in the absence of RelA. Silencing of both RelA and twist1 were additive leading to the highest expression of RelB. These data indicate that RelA expression in IPF fibroblasts is unrelated to twist1 and may even act as an inhibitor of RelB expression.

In these next experiments, we sought to determine if twist1 has a direct interaction with the promoter regions of CXCL12 and RelB. Twist1 binds to E-box motifs, CANNTG, and is most typically associated with transcriptional inhibition(41). Functional E-box motifs have been characterized upstream of the transcriptional start site for CXCL12 (35). To that end,

we first employed A549 cells in order to obtain an adequate number of cells for chromatin immunoprecipitation (ChIP). We show that A549 cells express twist1 (Figure 6H). For these experiments we scanned the regions directly upstream of the transcriptional start site for CXCL12 and RelB. E-box motifs were identified at the locations noted in Figure 6I. We hypothesized that we would detect possible interactions between twist1 and the E-boxes in these regions. To determine if the potential E-box motifs identified in the upstream sequences of CXCL12 and RelB gene bind to twist1, we conducted twist1 protein-specific ChIP assays and amplified the regions spanning these potential E-box motif site using multiple sets of primers (Table 2). PCR amplification (Figure 6J) was observed in both the input DNA as well as the flow-through fraction of the ChIP assay. As a control, no PCR amplification was observed after ChIP with non-immune mouse IgG1 or Rabbit IgG. Specific PCR products were detected only in the Twist Ab ChIP assay for the CXCL12 E4 and RelB E6+E7 sites. We then probed for these same sites in ChIP products from normal, IPF, and MRC5 lung fibroblasts (Figure 6K). We detected amplification of the CXCL12 E4 region in two of three normal lung fibroblasts sampled, all three IPF fibroblasts, and in the MRC5 cells. Amplification of the RelB E6–7 site was detected in all three normal lung fibroblasts and the MRC5 cells but in only one of three IPF fibroblasts. Therefore, these data suggest that twist1 interacts with E-box motifs within the promoter regions of CXCL12 and RelB.

Inhibition of CXCR4, the receptor for CXCL12, with AMD3100 blocks pulmonary fibrosis and accumulation of T-cells in twist1 FL mice

We have shown that the loss of twist1 leads to increased bleomycin-induced pulmonary fibrosis, possibly through a mechanism that involves expression of CXCL12 and the downstream recruitment of T-cells and bone marrow-derived matrix-producing cells to the lung. We next hypothesized that if the loss of twist1 drives increased expression of CXCL12 and pulmonary fibrosis in twist1 FL mice, then blockade of CXCL12 would protect from the exaggerated fibrosis. To test this hypothesis, first we determined the effect of twist1 silencing on expression of CXCR4, the receptor for CXCL12. First, we analyzed if bone marrow-derived COL1A2+ cells expressed CXCR4, a G-protein coupled receptor for CXCL12(42) (Figure S2A–E). Bone marrows from twist1 WT and twist1 FL mice were obtained at 14d after bleomycin injury or saline control. A small percentage of CD45+ bone marrow cells were tdTomato+ (Figure S2A–C). No significant differences were observed with injury or genotype. Of the CD45+tdTomato+ cells, greater than 95% of the cells were CXCR4+ (Figure S2A, B, D, E), and 40–50% of these cells were Ki67+, indicating that half of the CXCR4+ cells in the bone marrow are proliferating. No differences were observed between genotypes and injury. Next we determined CXCR4 expression in normal and IPF lung fibroblasts after silencing of twist1 by siRNA (Figure S2F–G). Following silencing of twist1, we found no effect on CXCR4 expression. These data show that CXCR4 is expressed on bone marrow-derived collagen-producing cells in mice and in human lung fibroblasts. Expression of CXCR4 is unaffected by twist1 expression.

In addition to CXCR4, CXCL12 also binds to CXCR7, but CXCR4 may mediate the more pro-fibrotic effects of CXCL12(43). Neutralization of CXCL12 signaling(44) and CXCR4 blockade by AMD3100 have been shown to decrease bleomycin-induced pulmonary fibrosis

(45). In this experiment, we treated bleomycin-injured or uninjured twist1 FL mice only with AMD3100 or a vehicle control (Figure 7). No effect of AMD3100 was observed in the absence of bleomycin injury. After bleomycin, significant injury and fibrosis was observed in the vehicle-treated mice (Figure 7A). This injury was largely absent from the AMD3100-treated bleomycin-injured twist1 FL mice. We determined the acid-soluble collagen content following injury (Figure 7B). Bleomycin injury was associated with a nearly fourfold increase in collagen content in the twist1 FL mice. Treatment with AMD3100 significantly blocked but did not completely reverse bleomycin-induced fibrosis in these mice. Next, we reasoned that if CXCL12 is responsible for the homing of inflammatory cells to the lung in the twist1 FL mice, then blockade of CXCR4 would block this accumulation. We then subjected the cells isolated from the BAL for flow cytometry to detect (Figure 7C–H) Ly6G, CD68, CD3, and B220 as described above for Figure 2. Following bleomycin injury, we found that AMD3100 significantly decreased the accumulation of CD3+ cells in the lung. These data suggest that blockade of CXCR4, the CXCL12 receptor, blocks the accumulation of T-cells in twist1 FL mice and partially blocks fibrosis. Additional reductions in Ly6G+ and CD68+ cells with AMD3100 treatment were also observed. AMD3100 may also block binding of MIF (Macrophage Migration Inhibitory Factor) to CXCR4(46). However, by quantitative RT-PCR, we found no significant difference in MIF expression from flow-sorted tdTomato+ cells from twist1 WT and twist1 FL animals (*data not shown*).

Low Twist1 Expression in IPF Is Associated with Enrichment of T-cell Pathways

We have shown that the loss of twist1 in the mesenchymal compartment in mice is associated with the accumulation of T-cells and enhanced bleomycin-induced pulmonary fibrosis. We next asked if the loss of twist1 in bleomycin injury can be modeled in actual IPF clinical data. To explore this question, we analyzed data from the LGRC as described in Materials and Methods. The LGRC cohort(47) is described in Table 2. These data combine gene expression analysis from whole lung homogenates with cross-sectional clinical data. We determined the relative expression for twist1 between IPF and controls (Figure 8A). Verifying our original data(3) in a new cohort, by microarray, from 134 patients with IPF compared to 108 normal controls, we found that twist1 was 2.3-fold increased in IPF. In addition, we have found that twist1 expression is increased in IPF compared to controls in an additional cohort (Figure S3A). These gene expression studies have employed whole lung homogenates. We subjected IPF and normal lung fibroblasts to immunoblotting for baseline twist1 expression in full media. We found that twist1 expression was higher in IPF fibroblasts compared to normal (Figure S3B). Because of the association of twist1 with CXCL12 and RelB, we queried the LGRC data for gene expression for these genes (Figure S3C–D). From whole lung, we found that CXCL12 goes up in IPF 1.5-fold ($P<0.001$) and that RelB goes down 30% ($P<0.05$). Next, we arranged the IPF patients into three equal tertiles based on increasing twist1 gene expression. In Figure 8B, twist1 expression increased from quartile 1 to 3 ($P=0.003$ for trend by one-way ANOVA, N=44–45 per tertile). Seeing a broad range of twist1 gene expression in this dataset, we hypothesized that IPF patients would be “transcriptomically” distinct based on twist1 gene expression. To test this hypothesis, we generated a heatmap of the IPF patients and arranged the patients in columns based on increasing twist1 expression (Figure 8C). Each of tertiles is marked by a break. Patients in tertile 1 were defined as “twist1-low,” and patients in tertile 3 were defined as

"twist1-high." With this analysis, we found that 387 genes (at a false discovery rate <0.05) were differentially expressed between the twist1-high and twist1-low patients. The 30 most up-regulated and most down-regulated genes are presented in Tables 3 and 4, respectively. We next subjected the differentially expressed gene list to Ingenuity Pathways Analysis (IPA). Table 5 is an analysis of the differentially-expressed genes and represents a calculation and a prediction whether certain pathways are activated or inhibited. These data suggest that patients in the twist1-low tertile are transcriptomically distinct from patients in the twist1-high tertile are characterized by activation of T-cell pathways downstream of IFNγ and STAT1. Taken together, twist1-low IPF patients and bleomycin-injured twist1 FL mice are characterized by enrichment of T-cell pathways.

While twist1-high and twist1-low patients are transcriptomically distinct, are they clinically distinct? We returned to the LGRC data and plotted forced vital capacity (FVC) and diffusing capacity for carbon monoxide (DLCO) as a function of twist1 expression (Figure 8D–E). We found that twist1 expression was not associated with FVC but was negatively associated with DLCO. Taken together, these data show that the transcriptomic differences between twist1-high and twist1-low patients are associated with a clinically relevant measure of gas exchange in IPF patients.

DISCUSSION

In this study, we tested the hypothesis that the loss of twist1 in the mesenchymal compartment would promote a fibroblast that is susceptible to apoptosis and thus protect these mice from pulmonary fibrosis. To our surprise, we found quite the opposite. Bleomycin-induced pulmonary fibrosis was exaggerated and characterized by T-cell dominant inflammation in the lung. To date, the association of twist1 with canonical NF-κB activity and chronic systemic inflammation in twist1 and twist2 heterozygous mice has been known (12). But our data show a very clear role for twist1 as a regulator of non-canonical NF-κB signaling and through CXCL12, leads to several potentially pro-fibrotic effects downstream. Increased CXCL12 in IPF fibroblasts is the result of de-repression of both CXCL12 and RelB transcription.

A relationship between twist1 and CXCL12 has recently been identified in cancer-associated fibroblasts (CAF) (48). The authors show that high expression of twist1 is associated with *increased* expression of CXCL12. These observations stand in contrast to our data where twist1 acts as a repressor of CXCL12 expression. The authors do show a decrease in CXCL12 luciferase activity with induction of twist1 in 293T cells, which would go along with our observation of twist1 as a transcriptional inhibitor. Increased CXCL12 in CAF may be related to other mechanisms not present in IPF lung fibroblasts. The increase in CXCL12 that we observed in IPF fibroblasts may be related principally to increased RelB. To our knowledge, this association between RelB and twist1 has not been described previously. In our system, we actually found that RelA, known to be a transcriptional regulator of RelB expression (49), appears to *inhibit* expression of RelB. Further study is needed to determine if this relationship in other inflammatory cells and the extent to which this mechanism may operate in other disease processes, where fibroblast-like cells are known to express CXCL12 such as rheumatoid arthritis and CAF (35, 50). These data support the concept that

mesenchymal cells in the lung are immunologically active and can act as potent regulators of the local inflammatory infiltrate with critical effects on phenotypes in the lung (36, 45, 51).

If the twist1 null mesenchymal cells enhance the accumulation of T-cells into the injured lung, to what extent is fibrosis driven by these T-cells? It is possible that the T-cell infiltrate may drive fibrosis as has been suggested previously (52). We recovered more CD4+ and CD8+ cells from bleomycin-injured twist1 FL animals compared to the twist1 WT controls. Th1 and Treg cells appeared to be most highly represented group amongst the CD4+ cells. All CD8 subphenotypes were more highly represented in the twist1 FL animals. But the implications of increased numbers of CD8+ cells in bleomycin injury and IPF in general are unclear. The data on the role of T-cells in animal models of fibrosis do not clearly identify whether they are pathologic or not. CXCL10 signaling appears to be protective against pulmonary fibrosis (53, 54). It should be noted that we did not detect altered expression of CXCL9, 10, or 11 in tdTomato+ cells isolated from bleomycin-injured mice (*data not shown*). Conversely, deficiency of Th1 cells may be deleterious. T-bet null mice have increased susceptibility to bleomycin injury (55) suggesting a positive role for Th1 cells in this model. In contrast, *loss* of T regulatory CD4+CD25+ cells protected against bleomycin injury (56). This suggests that the balance of CD4+ cell sub-phenotypes is crucial to regulating pulmonary fibrosis. Future studies to deplete T-cells in twist1 FL mice or simultaneous conditional knockout of CXCL12 may determine to what extent T-cells are necessary for the increased fibrosis observed in bleomycin-injured twist1 FL mice.

Finally, we have found that a cohort of IPF patients with low expression of twist1 is characterized by activation of T-cell pathways. This is entirely consistent with our experimental model where loss of twist1 in the mesenchymal compartment is associated with accumulation of T-cells. But we are left to reconcile what appears to be a paradox between the animal model and IPF: The animal is worse, but is the IPF patient “better?” We can only speculate if the twist1-low IPF patient is indeed “better” for several reasons. First, the LGRC data are cross-sectional, so the outcomes for these patients are unknown. It would seem that enhancement of inflammation as exemplified in the twist1 low patient would be a negative prognostic factor in IPF and might contribute to reduced survival. Second, while the difference in DLCO between the tertiles suggests that that the transcriptomic distinctiveness of twist1-high and twist1-low patients is associated with an actual clinical phenotype, the lack of association of twist1 with forced vital capacity (FVC) (57)—the most reproducible measure of prognosis in IPF—may argue against the idea that twist1-low patients are healthier. Third, we have modeled loss of twist1 in the mesenchymal compartment. However, because the LGRC data are from whole lung gene expression, the cell or cells that express twist1 at a low level are unknown. Future studies, perhaps with single cell RNASeq from suspensions of whole IPF lungs may provide the granularity to correlate twist1 with CXCL12 and RelB *in vivo*. While epithelial cells are potentially an important cell type to study in the context of twist1 expression, it has recently been found that epithelial cell-specific loss of twist1 does not have a fibrosis phenotype (58). The association of twist1 with DLCO may also argue for a pulmonary vascular phenotype as may be suggested by experimental data with adventitial fibroblasts (36, 51). Further evidence in support of the association of twist1 with a pulmonary vascular phenotype comes from recent data that show that knockout of twist1 in endothelial cells is protective from bleomycin injury(59).

Inflammation may be reduced in with loss of twist1 in endothelial cells, which may, in part, explain the protection from bleomycin injury that the authors observed. Finally, this apparent paradox between our observations in mice and in patients highlights the contrasts between bleomycin injury in mice and IPF. We suggest that the critical observation from our experimental data is the effect of T-cell activation on the phenotype of bleomycin-injured mice and IPF patients. Further study is needed to understand the role of twist1 in other compartments in the lung in other experimental models of pulmonary fibrosis in addition to the role that inflammation plays in IPF.

IPF is a disease classically defined as *independent* of inflammation(60). However, in studies of both experimental and idiopathic pulmonary fibrosis (29, 52, 61–64), there is now increased recognition of the role that inflammation can play (65). We have found that the loss of twist1 in the mesenchymal compartment in mice leads to increased expression of CXCL12, which promotes crosstalk with and accumulation of T-cells in the lung and increased pulmonary fibrosis. Twist1 may be one of the factors that shape the fibrotic phenotype in IPF and in experimental lung injury.

Supplementary Material

Refer to Web version on PubMed Central for supplementary material.

Acknowledgments

This project was supported by the Simmons Center for Interstitial Lung Disease, R01HL095397 and RC2HL101715 (NK), DK104680-01A1 (PSB), and R01HL126990 (DJK). The Human Airway Cell and Tissue Core (072506) and the Human Airway Cell and Tissue Core (Cystic Fibrosis Foundation Research Development Program Grant), under the direction of Joseph Pilewski and Mauricio Rojas, provided human lung fibroblasts.

WORKS CITED

1. Thannickal VJ, Horowitz JC. Evolving concepts of apoptosis in idiopathic pulmonary fibrosis. Proc Am Thorac Soc. 2006; 3:350–356. [PubMed: 16738200]
2. Lawson WE, Crossno PF, Polosukhin VV, Roldan J, Cheng DS, Lane KB, Blackwell TR, Xu C, Markin C, Ware LB, Miller GG, Loyd JE, Blackwell TS. Endoplasmic reticulum stress in alveolar epithelial cells is prominent in IPF: association with altered surfactant protein processing and herpesvirus infection. American journal of physiology Lung cellular and molecular physiology. 2008; 294:L1119–1126. [PubMed: 18390830]
3. Bridges RS, Kass D, Loh K, Glackin C, Borczuk AC, Greenberg S. Gene expression profiling of pulmonary fibrosis identifies Twist1 as an antiapoptotic molecular “rectifier” of growth factor signaling. Am J Pathol. 2009; 175:2351–2361. [PubMed: 19893041]
4. Ajayi IO, Sisson TH, Higgins PD, Booth AJ, Sagana RL, Huang SK, White ES, King JE, Moore BB, Horowitz JC. X-linked inhibitor of apoptosis regulates lung fibroblast resistance to Fas-mediated apoptosis. American journal of respiratory cell and molecular biology. 2013; 49:86–95. [PubMed: 23492187]
5. Parker MW, Rossi D, Peterson M, Smith K, Sikstrom K, White ES, Connett JE, Henke CA, Larsson O, Bitterman PB. Fibrotic extracellular matrix activates a profibrotic positive feedback loop. J Clin Invest. 2014; 124:1622–1635. [PubMed: 24590289]
6. Gao Z, Sasaoka T, Fujimori T, Oya T, Ishii Y, Sabit H, Kawaguchi M, Kurotaki Y, Naito M, Wada T, Ishizawa S, Kobayashi M, Nabeshima Y, Sasahara M. Deletion of the PDGFR-beta gene affects key fibroblast functions important for wound healing. The Journal of biological chemistry. 2005; 280:9375–9389. [PubMed: 15590688]

7. Xia H, Khalil W, Kahm J, Jessurun J, Kleidon J, Henke CA. Pathologic caveolin-1 regulation of PTEN in idiopathic pulmonary fibrosis. Am J Pathol. 176:2626–2637.
8. Xia H, Diebold D, Nho R, Perlman D, Kleidon J, Kahm J, Avdulov S, Peterson M, Nerva J, Bitterman P, Henke C. Pathological integrin signaling enhances proliferation of primary lung fibroblasts from patients with idiopathic pulmonary fibrosis. The Journal of experimental medicine. 2008; 205:1659–1672. [PubMed: 18541712]
9. Thisse B, el Messal M, Perrin-Schmitt F. The twist gene: isolation of a Drosophila zygotic gene necessary for the establishment of dorsoventral pattern. Nucleic Acids Res. 1987; 15:3439–3453. [PubMed: 3106932]
10. Howard TD, Paznekas WA, Green ED, Chiang LC, Ma N, Ortiz de Luna RI, Garcia Delgado C, Gonzalez-Ramos M, Kline AD, Jabs EW. Mutations in TWIST, a basic helix-loop-helix transcription factor, in Saethre-Chotzen syndrome. Nat Genet. 1997; 15:36–41. [PubMed: 8988166]
11. Chen ZF, Behringer RR. twist is required in head mesenchyme for cranial neural tube morphogenesis. Genes Dev. 1995; 9:686–699. [PubMed: 7729687]
12. Sosic D, Richardson JA, Yu K, Ornitz DM, Olson EN. Twist regulates cytokine gene expression through a negative feedback loop that represses NF-kappaB activity. Cell. 2003; 112:169–180. [PubMed: 12553906]
13. Okada T, Sugie I, Aisaka K. Effects of gamma-interferon on collagen and histamine content in bleomycin-induced lung fibrosis in rats. Lymphokine Cytokine Res. 1993; 12:87–91. [PubMed: 7686780]
14. Cheng GZ, Chan J, Wang Q, Zhang W, Sun CD, Wang LH. Twist transcriptionally up-regulates AKT2 in breast cancer cells leading to increased migration, invasion, and resistance to paclitaxel. Cancer research. 2007; 67:1979–1987. [PubMed: 17332325]
15. Karreth F, Tuveson DA. Twist induces an epithelial-mesenchymal transition to facilitate tumor metastasis. Cancer Biol Ther. 2004; 3:1058–1059. [PubMed: 15640618]
16. Pozharskaya V, Torres-Gonzalez E, Rojas M, Gal A, Amin M, Dollard S, Roman J, Stecenko AA, Mora AL. Twist: a regulator of epithelial-mesenchymal transition in lung fibrosis. PLoS One. 2009; 4:e7559. [PubMed: 19851501]
17. Zheng B, Zhang Z, Black CM, de Crombrugghe B, Denton CP. Ligand-dependent genetic recombination in fibroblasts : a potentially powerful technique for investigating gene function in fibrosis. The American journal of pathology. 2002; 160:1609–1617. [PubMed: 12000713]
18. Bialek P, Kern B, Yang X, Schrock M, Sosic D, Hong N, Wu H, Yu K, Ornitz DM, Olson EN, Justice MJ, Karsenty G. A twist code determines the onset of osteoblast differentiation. Developmental cell. 2004; 6:423–435. [PubMed: 15030764]
19. Devor DC, Bridges RJ, Pilewski JM. Pharmacological modulation of ion transport across wild-type and DeltaF508 CFTR-expressing human bronchial epithelia. American journal of physiology Cell physiology. 2000; 279:C461–479. [PubMed: 10913013]
20. Pilewski JM, Liu L, Henry AC, Knauer AV, Feghali-Bostwick CA. Insulin-like growth factor binding proteins 3 and 5 are overexpressed in idiopathic pulmonary fibrosis and contribute to extracellular matrix deposition. The American journal of pathology. 2005; 166:399–407. [PubMed: 15681824]
21. Kass D, Bridges RS, Borczuk A, Greenberg S. Methionine aminopeptidase-2 as a selective target of myofibroblasts in pulmonary fibrosis. American journal of respiratory cell and molecular biology. 2007; 37:193–201. [PubMed: 17446530]
22. Shu HK, Yoon Y, Hong S, Xu K, Gao H, Hao C, Torres-Gonzalez E, Nayra C, Rojas M, Shim H. Inhibition of the CXCL12/CXCR4-axis as preventive therapy for radiation-induced pulmonary fibrosis. PLoS One. 2013; 8:e79768. [PubMed: 24244561]
23. Ramani K, Garg AV, Jawale CV, Conti HR, Whibley N, Jackson EK, Shiva SS, Horne W, Kolls JK, Gaffen SL, Biswas PS. The Kallikrein-Kinin System: A Novel Mediator of IL-17-Driven Anti-Candida Immunity in the Kidney. PLoS Pathog. 2016; 12:e1005952. [PubMed: 27814401]
24. Ramani K, Pawaria S, Maers K, Huppler AR, Gaffen SL, Biswas PS. An essential role of interleukin-17 receptor signaling in the development of autoimmune glomerulonephritis. J Leukoc Biol. 2014; 96:463–472. [PubMed: 24935958]

25. Kass DJ, Yu G, Loh KS, Savir A, Borczuk A, Kahloon R, Juan-Guardela B, Deiuliis G, Tedrow J, Choi J, Richards T, Kaminski N, Greenberg SM. Cytokine-like factor 1 gene expression is enriched in idiopathic pulmonary fibrosis and drives the accumulation of CD4+ T cells in murine lungs: evidence for an antifibrotic role in bleomycin injury. The American Journal of P athology. 2012; 180:1963–1978.
26. Yu S, Yerges-Armstrong LM, Chu Y, Zmuda JM, Zhang Y. AP2 suppresses osteoblast differentiation and mineralization through down-regulation of Frizzled-1. Biochem J. 2015; 465:395–404. [PubMed: 25369469]
27. Yu S, Yerges-Armstrong LM, Chu Y, Zmuda JM, Zhang Y. E2F1 effects on osteoblast differentiation and mineralization are mediated through up-regulation of frizzled-1. Bone. 2013; 56:234–241. [PubMed: 23806799]
28. Bauer Y, Tedrow J, de Bernard S, Birker-Robaczewska M, Gibson KF, Guardela BJ, Hess P, Klenk A, Lindell KO, Poirey S, Renault B, Rey M, Weber E, Nayler O, Kaminski N. A novel genomic signature with translational significance for human idiopathic pulmonary fibrosis. Am J Respir Cell Mol Biol. 2015; 52:217–231. [PubMed: 25029475]
29. Herazo-Maya JD, Noth I, Duncan SR, Kim S, Ma SF, Tseng GC, Feingold E, Juan-Guardela BM, Richards TJ, Lussier Y, Huang Y, Vij R, Lindell KO, Xue J, Gibson KF, Shapiro SD, Garcia JG, Kaminski N. Peripheral blood mononuclear cell gene expression profiles predict poor outcome in idiopathic pulmonary fibrosis. Sci Transl Med. 2013; 5:205ra136.
30. Wu W, Dave N, Tseng GC, Richards T, Xing EP, Kaminski N. Comparison of normalization methods for CodeLink Bioarray data. BMC bioinformatics. 2005; 6:309. [PubMed: 16381608]
31. Konishi K, Gibson KF, Lindell KO, Richards TJ, Zhang Y, Dhir R, Bisceglia M, Gilbert S, Yousem SA, Song JW, Kim DS, Kaminski N. Gene expression profiles of acute exacerbations of idiopathic pulmonary fibrosis. Am J Respir Crit Care Med. 2009; 180:167–175. [PubMed: 19363140]
32. Rock JR, Barkauskas CE, Cronce MJ, Xue Y, Harris JR, Liang J, Noble PW, Hogan BL. Multiple stromal populations contribute to pulmonary fibrosis without evidence for epithelial to mesenchymal transition. Proceedings of the National Academy of Sciences of the United States of America. 2011; 108:E1475–1483. [PubMed: 22123957]
33. Phillips RJ, Burdick MD, Hong K, Lutz MA, Murray LA, Xue YY, Belperio JA, Keane MP, Strieter RM. Circulating fibrocytes traffic to the lungs in response to CXCL12 and mediate fibrosis. The Journal of clinical investigation. 2004; 114:438–446. [PubMed: 15286810]
34. Hashimoto N, Jin H, Liu T, Chensue SW, Phan SH. Bone marrow-derived progenitor cells in pulmonary fibrosis. The Journal of Clinical Investigation. 2004; 113:243–252. [PubMed: 14722616]
35. Santiago B, Calonge E, Del Rey MJ, Gutierrez-Canas I, Izquierdo E, Usategui A, Galindo M, Alcami J, Pablos JL. CXCL12 gene expression is upregulated by hypoxia and growth arrest but not by inflammatory cytokines in rheumatoid synovial fibroblasts. Cytokine. 2011; 53:184–190. [PubMed: 20609598]
36. Li M, Riddle SR, Frid MG, El Kasmi KC, McKinsey TA, Sokol RJ, Strassheim D, Meyrick B, Yeager ME, Flockton AR, McKeon BA, Lemon DD, Horn TR, Anwar A, Barajas C, Stenmark KR. Emergence of fibroblasts with a proinflammatory epigenetically altered phenotype in severe hypoxic pulmonary hypertension. J Immunol. 2011; 187:2711–2722. [PubMed: 21813768]
37. Madge LA, May MJ. Classical NF-kappaB activation negatively regulates noncanonical NF-kappaB-dependent CXCL12 expression. The Journal of biological chemistry. 2010; 285:38069–38077. [PubMed: 20923761]
38. Sun SC. The noncanonical NF-kappaB pathway. Immunol Rev. 2012; 246:125–140. [PubMed: 22435551]
39. Lee FS, Peters RT, Dang LC, Maniatis T. MEKK1 activates both IkappaB kinase alpha and IkappaB kinase beta. Proceedings of the National Academy of Sciences of the United States of America. 1998; 95:9319–9324. [PubMed: 9689078]
40. Millet P, McCall C, Yoza B. RelB: an outlier in leukocyte biology. J Leukoc Biol. 2013; 94:941–951. [PubMed: 23922380]

41. Laursen KB, Mielke E, Iannaccone P, Fuchtbauer EM. Mechanism of transcriptional activation by the proto-oncogene Twist1. The Journal of biological chemistry. 2007; 282:34623–34633. [PubMed: 17893140]

42. Balabanian K, Lagane B, Infantino S, Chow KY, Harriague J, Moepps B, Arenzana-Seisdedos F, Thelen M, Bachelerie F. The chemokine SDF-1/CXCL12 binds to and signals through the orphan receptor RDC1 in T lymphocytes. The Journal of biological chemistry. 2005; 280:35760–35766. [PubMed: 16107333]

43. Ding BS, Cao Z, Lis R, Nolan DJ, Guo P, Simons M, Penfold ME, Shido K, Rabbany SY, Rafii S. Divergent angiocrine signals from vascular niche balance liver regeneration and fibrosis. Nature. 2014; 505:97–102. [PubMed: 24256728]

44. Xu J, Mora A, Shim H, Stecenko A, Brigham KL, Rojas M. Role of the SDF-1/CXCR4 axis in the pathogenesis of lung injury and fibrosis. American journal of respiratory cell and molecular biology. 2007; 37:291–299. [PubMed: 17463394]

45. Song JS, Kang CM, Kang HH, Yoon HK, Kim YK, Kim KH, Moon HS, Park SH. Inhibitory effect of CXC chemokine receptor 4 antagonist AMD3100 on bleomycin induced murine pulmonary fibrosis. Exp Mol Med. 2010; 42:465–472. [PubMed: 20498529]

46. Schwartz V, Kruttgen A, Weis J, Weber C, Ostendorf T, Lue H, Bernhagen J. Role for CD74 and CXCR4 in clathrin-dependent endocytosis of the cytokine MIF. Eur J Cell Biol. 2012; 91:435–449. [PubMed: 22014447]

47. Tan J, Tedrow JR, Dutta JA, Juan-Guardela B, Nouraie M, Chu Y, Trejo Bittar H, Ramani K, Biswas PS, Veraldi KL, Kaminski N, Zhang Y, Kass DJ. Expression of RXFP1 is Decreased in Idiopathic Pulmonary Fibrosis: Implications for Relaxin-Based Therapies. Am J Respir Crit Care Med. 2016

48. Lee KW, Yeo SY, Sung CO, Kim SH. Twist1 is a key regulator of cancer-associated fibroblasts. Cancer Res. 2015; 75:73–85. [PubMed: 25368021]

49. Bren GD, Solan NJ, Miyoshi H, Pennington KN, Pobst LJ, Paya CV. Transcription of the RelB gene is regulated by NF-kappaB. Oncogene. 2001; 20:7722–7733. [PubMed: 11753650]

50. Kojima Y, Acar A, Eaton EN, Mellody KT, Scheel C, Ben-Porath I, Onder TT, Wang ZC, Richardson AL, Weinberg RA, Orimo A. Autocrine TGF-beta and stromal cell-derived factor-1 (SDF-1) signaling drives the evolution of tumor-promoting mammary stromal myofibroblasts. Proc Natl Acad Sci U S A. 2010; 107:20009–20014. [PubMed: 21041659]

51. Frid MG, Li M, Gnanasekharan M, Burke DL, Fragoso M, Strassheim D, Sylman JL, Stenmark KR. Sustained hypoxia leads to the emergence of cells with enhanced growth, migratory, and promitogenic potentials within the distal pulmonary artery wall. American journal of physiology Lung cellular and molecular physiology. 2009; 297:L1059–1072. [PubMed: 19767409]

52. Reilkoff RA, Peng H, Murray LA, Peng X, Russell T, Montgomery R, Feghali-Bostwick C, Shaw A, Homer RJ, Gulati M, Mathur A, Elias JA, Herzog EL. Semaphorin 7a+ regulatory T cells are associated with progressive idiopathic pulmonary fibrosis and are implicated in transforming growth factor-beta1-induced pulmonary fibrosis. Am J Respir Crit Care Med. 2013; 187:180–188. [PubMed: 23220917]

53. Jiang D, Liang J, Hodge J, Lu B, Zhu Z, Yu S, Fan J, Gao Y, Yin Z, Homer R, Gerard C, Noble PW. Regulation of pulmonary fibrosis by chemokine receptor CXCR3. J Clin Invest. 2004; 114:291–299. [PubMed: 15254596]

54. Jiang D, Liang J, Campanella GS, Guo R, Yu S, Xie T, Liu N, Jung Y, Homer R, Meltzer EB, Li Y, Tager AM, Goetinck PF, Luster AD, Noble PW. Inhibition of pulmonary fibrosis in mice by CXCL10 requires glycosaminoglycan binding and syndecan-4. J Clin Invest. 2010; 120:2049–2057. [PubMed: 20484822]

55. Xu J, Mora AL, LaVoy J, Brigham KL, Rojas M. Increased bleomycin-induced lung injury in mice deficient in the transcription factor T-bet. Am J Physiol Lung Cell Mol Physiol. 2006; 291:L658–667. [PubMed: 16648243]

56. Boveda-Ruiz D, D'Alessandro-Gabazza CN, Toda M, Takagi T, Naito M, Matsushima Y, Matsumoto T, Kobayashi T, Gil-Bernabe P, Chelakkot-Govindalayathil AL, Miyake Y, Yasukawa A, Morser J, Taguchi O, Gabazza EC. Differential role of regulatory T cells in early and late stages of pulmonary fibrosis. Immunobiology. 2013; 218:245–254. [PubMed: 22739236]

57. du Bois RM, Weycker D, Albera C, Bradford WZ, Costabel U, Kartashov A, King TE Jr, Lancaster L, Noble PW, Sahn SA, Thomeer M, Valeyre D, Wells AU. Forced vital capacity in patients with idiopathic pulmonary fibrosis: test properties and minimal clinically important difference. Am J Respir Crit Care Med. 2011; 184:1382–1389. [PubMed: 21940789]
58. Yang J, Velikoff M, Agarwal M, Disayabutr S, Wolters PJ, Kim KK. Overexpression of inhibitor of DNA-binding 2 attenuates pulmonary fibrosis through regulation of c-Abl and Twist. Am J Pathol. 2015; 185:1001–1011. [PubMed: 25661109]
59. Mammoto T, Jiang A, Jiang E, Mammoto A. Role of Twist1 Phosphorylation in Angiogenesis and Pulmonary Fibrosis. Am J Respir Cell Mol Biol. 2016; 55:633–644. [PubMed: 27281171]
60. Selman M, King TE, Pardo A. S. American Thoracic, S. European Respiratory, and P. American College of Chest. Idiopathic pulmonary fibrosis: prevailing and evolving hypotheses about its pathogenesis and implications for therapy. Ann Intern Med. 2001; 134:136–151. [PubMed: 11177318]
61. Xue J, Kass DJ, Bon J, Vuga L, Tan J, Csizmadia E, Otterbein L, Soejima M, Levesque MC, Gibson KF, Kaminski N, Pilewski JM, Donahoe M, Sciurba FC, Duncan SR. Plasma B lymphocyte stimulator and B cell differentiation in idiopathic pulmonary fibrosis patients. J Immunol. 2013; 191:2089–2095. [PubMed: 23872052]
62. Prasse A, Probst C, Bargagli E, Zissel G, Toews GB, Flaherty KR, Olschewski M, Rottoli P, Muller-Quernheim J. Serum CC-chemokine ligand 18 concentration predicts outcome in idiopathic pulmonary fibrosis. Am J Respir Crit Care Med. 2009; 179:717–723. [PubMed: 19179488]
63. Luzina IG, Kopach P, Lockatell V, Kang PH, Nagarsekar A, Burke AP, Hasday JD, Todd NW, Atamas SP. Interleukin-33 potentiates bleomycin-induced lung injury. Am J Respir Cell Mol Biol. 2013; 49:999–1008. [PubMed: 23837438]
64. Donahoe M V, Valentine G, Chien N, Gibson KF, Raval JS, Saul M, Xue J, Zhang Y, Duncan SR. Autoantibody-Targeted Treatments for Acute Exacerbations of Idiopathic Pulmonary Fibrosis. PLoS One. 2015; 10:e0127771. [PubMed: 26083430]
65. King TE Jr, Pardo A, Selman M. Idiopathic pulmonary fibrosis. Lancet. 2011; 378:1949–1961. [PubMed: 21719092]

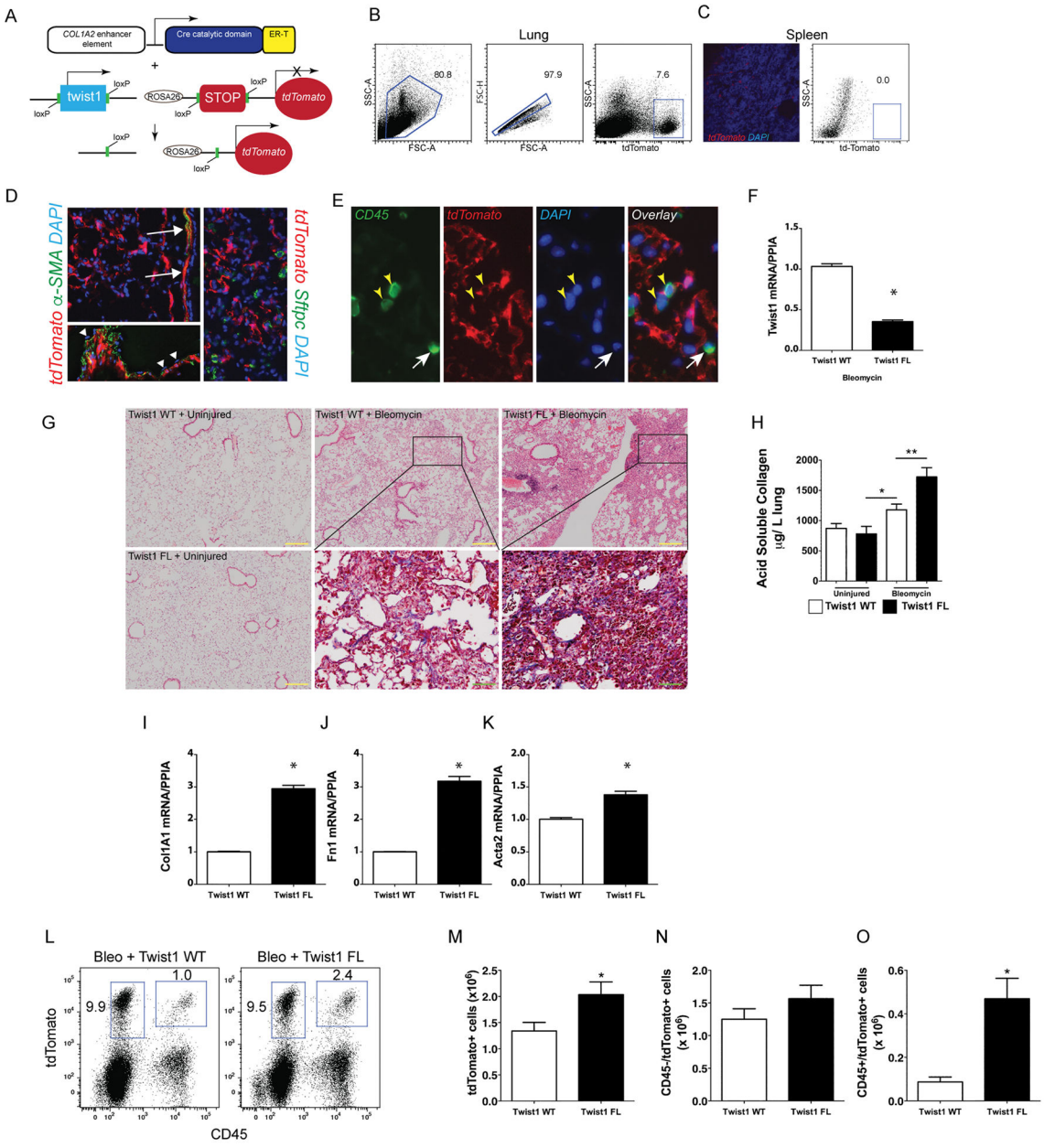

Figure 1. Loss of twist1 in *COL1A2*+ cells leads to increased bleomycin-induced pulmonary fibrosis

(A) Schematic representation of triple transgenic *COL1A2* cre-ER(T) *twist1 fl/fl* ROSA26-tdTomato mouse (Twist1 FL). (B) Gating strategy for tdTomato+ cells in the lung. (C) Negative control fluorescent images of spleen showing rare tdTomato+ cells (*left)* and dot plots of splenocytes showing absence of tdTomato+ cells (*right*). (D) Fluorescent images of lungs from bleomycin-injured animals showing tdTomato+ (*red*) cells and staining alpha-SMA (*left, green)* or SFTPC (right, *green*), magnification ×200. Arrows show alpha-SMA +tdTomato+ airway vascular muscle. Arrowheads show tdTomato- endothelial cells overlying vascular smooth muscle. Nuclei are counterstained with DAPI. (E) Immunofluorescent images of CD45 expression (*green*). Yellow arrowheads identify

CD45+tdTomato+ cells and the white arrow identifies a CD45+tdTomato- cell, magnification ×400. (F) At 14d after injury, tdTomato+ cells from twist1 WT or twist1 FL injured with bleomycin were flow-sorted and processed immediately for quantitative RT-PCR of twist1 (*P<0.0001, N=3). (G) Hematoxylin and eosin staining of lungs at 14d after bleomycin injury in twist1 WT or twist1 FL animals (Yellow inset bar=200μm, magnification ×100). Masson's trichrome images from bleomycin-injured are magnified (Green inset bar=50μm, magnification ×400). (H) Left lungs were processed for detection of acid soluble collagen. Bleomycin-induced deposition of collagen was increased in twist1 FL animals compared to WT controls (P<0.003, Bleo + twist1 WT v Bleo + twist1 FL, by ANOVA, N=10–14 per group). Quantitative RT-PCR of flow-sorted cells from bleomycin injured twist1 WT or FL animals for (I) COL1A1 (*P<0.0001, N=3 by t-test), (J) FN1 (*P=0.0001, N=3 by t-test), and (K) Acta2 (α-smooth muscle actin, *P=0.033, N=3 by t-test). (L–M) Flow cytometry was performed to quantify the number of CD45+ and tdTomato + cells. Total tdTomato+ cells were significantly higher in the bleomycin-injured twist1 FL mice than their WT counterparts. (P<0.04, N=8–9). No significant difference was observed between tdTomato+ CD45− cells in (N). (O) Significantly more CD45+tdTomato+ cells were detected in the twist1 FL animals than in the WT (P=0.002, N=8–9).

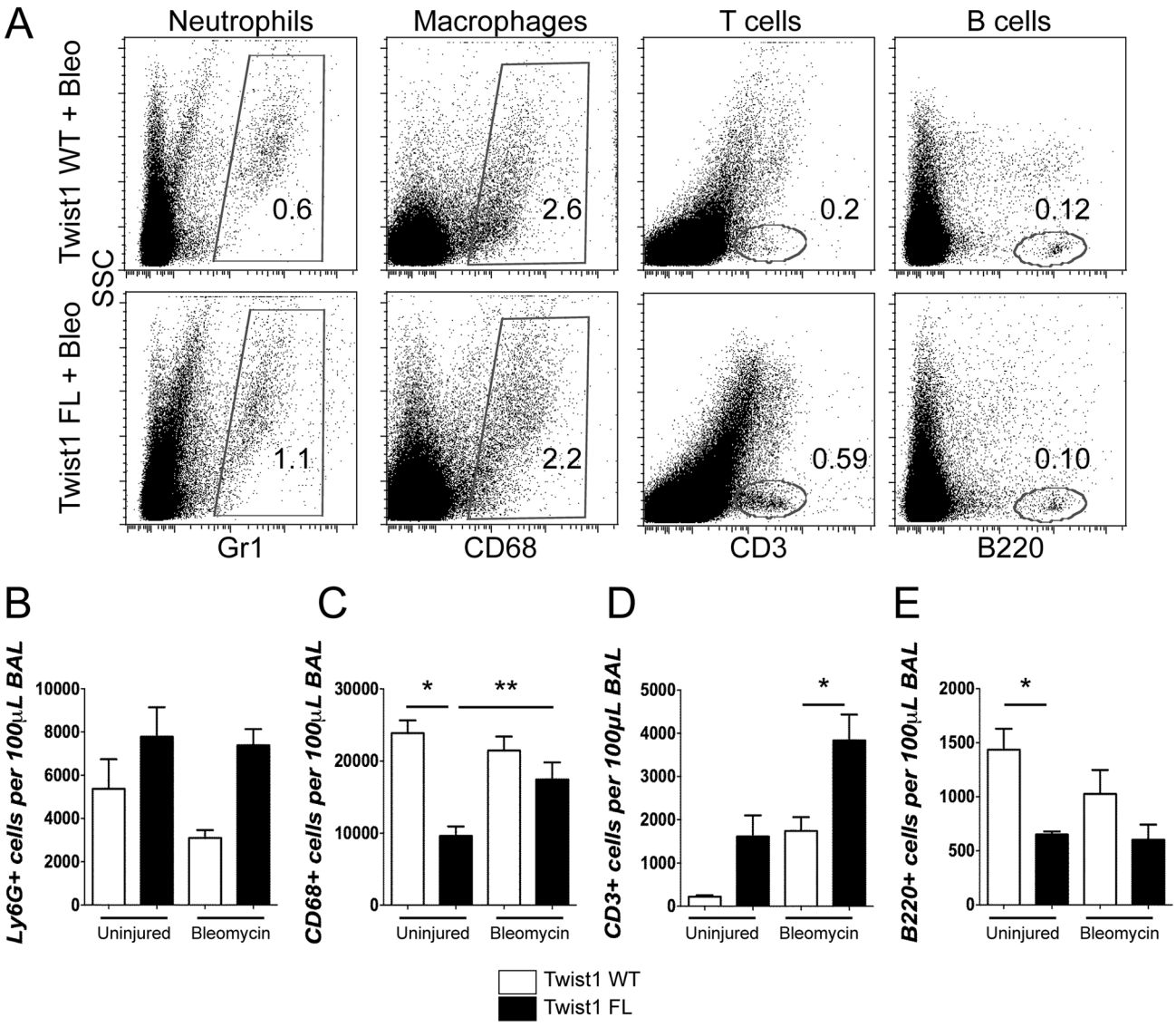

Figure 2. Loss of twist1 in COL1A2+ cells is associated with enhanced accumulation of T-cells following bleomycin injury

Bronchoalveolar lavage (BAL)was processed for flow cytometry for markers of neutrophils, macrophages, and T- and B-cells (A–E). For these experiments, N=5 per uninjured condition and 11–12 for injured conditions. BAL was collected at 14d after injury. (A) Dot plots of uninjured and bleomycin-injured animals for neutrophils, macrophages, T-cells, and B-cells. Quantification of (B) Ly6G, (C) CD68 (*P=0.006, Uninjured Twist1 WT v Uninjured Twist1 FL, and **P<0.025 by ANOVA, Uninjured+Twist1 FL v Bleomycin+Twist1 FL), (D) CD3 (*P=0.0021, Bleomycin+Twist1 WT v Bleomycin +Twist1 FL), and (E) B220 (*P=0.03, Uninjured+Twist1 WT v Uninjured + Twist1 FL).

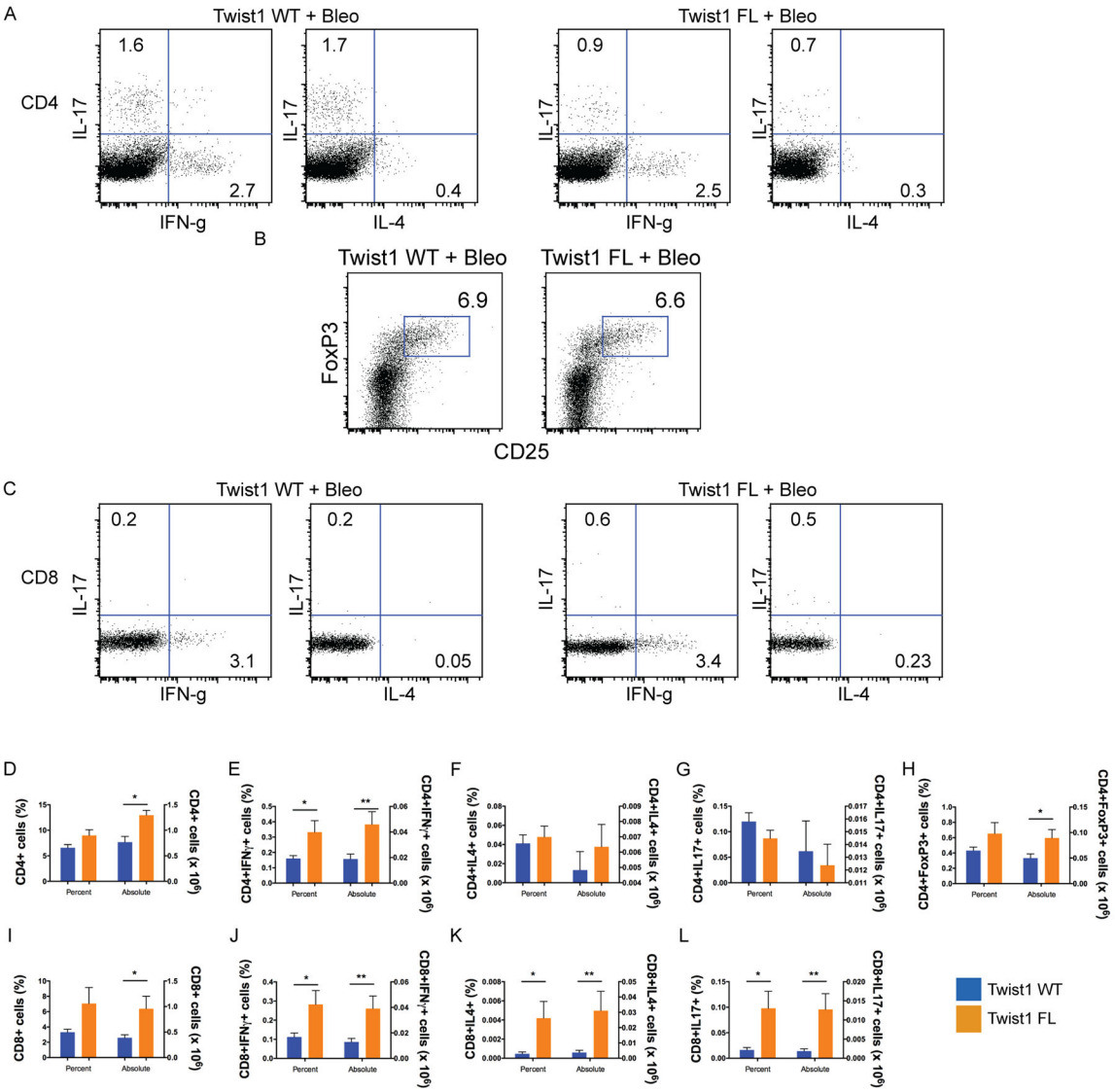

Figure 3. Subphenotyping of T-cells from bleomycin-injured Twist1 FL and WT mice

Flow cytometry of single cell suspensions of bleomycin-injured Twist1 WT or Twist1 FL mouse lungs to describe the T-cell subphenotypes following stimulation and intracellular cytokine staining as described in Materials and Methods. (A) Dot plots for CD4+ IFNg, IL-4, and IL-17 from bleomycin-injured Twist1 WT and Twist1 FL animals. (B) Dot plot for CD4+Foxp3+ cells. (C) Dot plots for CD8+ IFNg, IL-4, and IL-17. Percentage of cells (*left y axis*) and the absolute numbers of cells (*right y axis*) are reported, N=8 per condition and data were analyzed by unpaired t-test. (D) CD4 (*P=0.003). (E) CD4+IFNγ (*P=0.04, **P=0.02). (F) CD4+IL4. (G) CD4+IL17. (H) CD4+Foxp3 (*P<0.05). (I) CD8 (*P=0.04). (J) CD8+IFNγ (*P=0.04, **P=0.03). (K) CD8+IL4 (*P<0.05, **P=0.05). (L) CD8+IL17, (*P<0.03, **P=0.02).

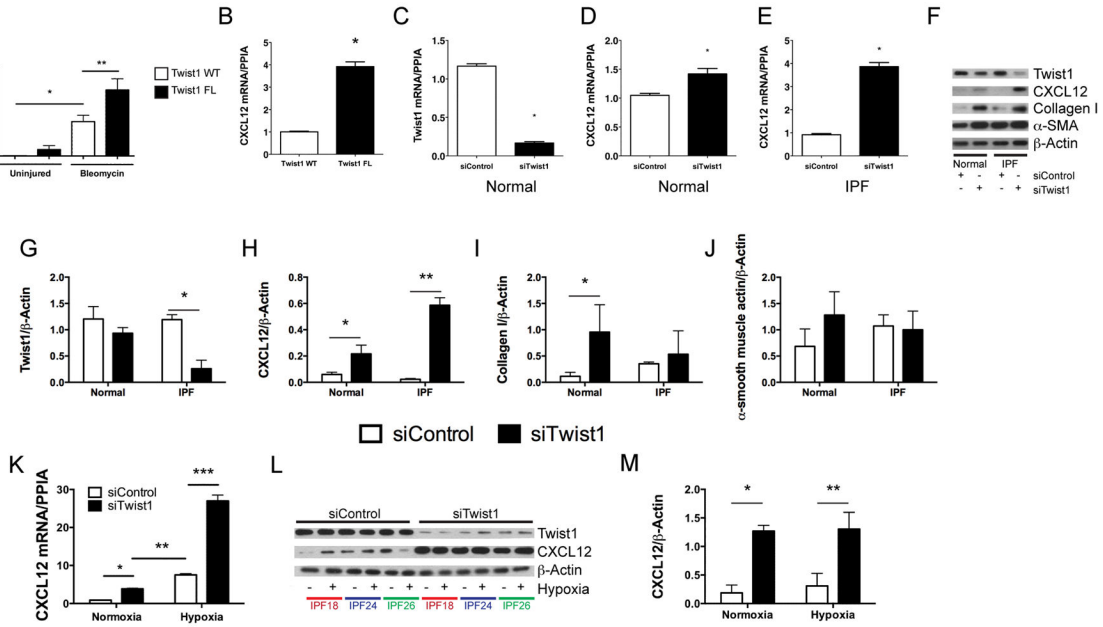

Figure 4. Loss of twist1 in COL1A2+ cells and in human lung fibroblasts leads to increased expression of CXCL12

(A) Bronchoalveolar lavage from twist1 WT and twist 1 FL animals at 14d following bleomycin injury was analyzed by ELISA for CXCL12 as described in Materials and Methods (*P<0.002, N=5–8, twist1 WT + uninjured v twist1 WT + bleomycin; **P<0.004, twist1 WT + bleomycin v twist1 FL + bleomycin, N=4–5 per group). (B) Quantitative RT PCR for CXCL12 was performed on tdTomato+ cells flow-sorted from twist1 WT or twist1 FL animals following bleomycin injury (*P<0.0002, by t-test, N=3). Normal human lung fibroblasts were cultured in the presence of twist1 siRNA (siTwist1) or non-targeting controls (siControl) and processed for quantitative RT-PCR for (C) twist (*P<0.0001, by t-test, N=3) and for (D) CXCL12 (*P<0.022, by t-test, N=3). (D) IPF-derived lung fibroblasts were also treated with siTwist1 or siControl, and qPCR was performed for CXCL12 (*P<0.0001, by t-test, N=3). (F) Normal and IPF lung fibroblasts were incubated with siTwist1 or siControl and subjected to immunoblotting for twist1, CXCL12, Collagen I, and α-SMA. All experiments reflect fibroblasts from three independent normal and three IPF lungs. Data were analyzed by two-way ANOVA followed by Neuman-Keuls post-hoc testing. Band intensity was quantified for (G) twist1 (*P<0.0001 IPF siTwist1 v siControl, N=3), (H) CXCL12 (*P<0.03 Normal siTwist1 v siControl, N=3 and **P<0.0001 IPF siTwist1 v siControl, N=3 (I) Collagen I (*P<0.02, Normal siTwist1 v siControl, N=3), and (J) α-SMA. (K) Quantitative RT-PCR for CXCL12 was performed on IPF lung fibroblasts in the presence of siControl or siTwist1 with and without hypoxia (*P<0.03 IPF siTwist1 v siControl under normoxic conditions, and **P<0.0003 IPF normoxia and hypoxia, and ***P<0.0001, siControl v siTwist1 under hypoxic conditions, N=3). (L) Immunoblot for twist1 and CXCL12 with siControl or siTwist1 in the presence or absence of hypoxia. (M) ImageJ quantification of the blots in (L) for CXCl12 (*P<0.0002 IPF siControl v siTwist1 in normoxia and **P<0.0001, siControl v siTwist1 under hypoxic conditions, N=3).

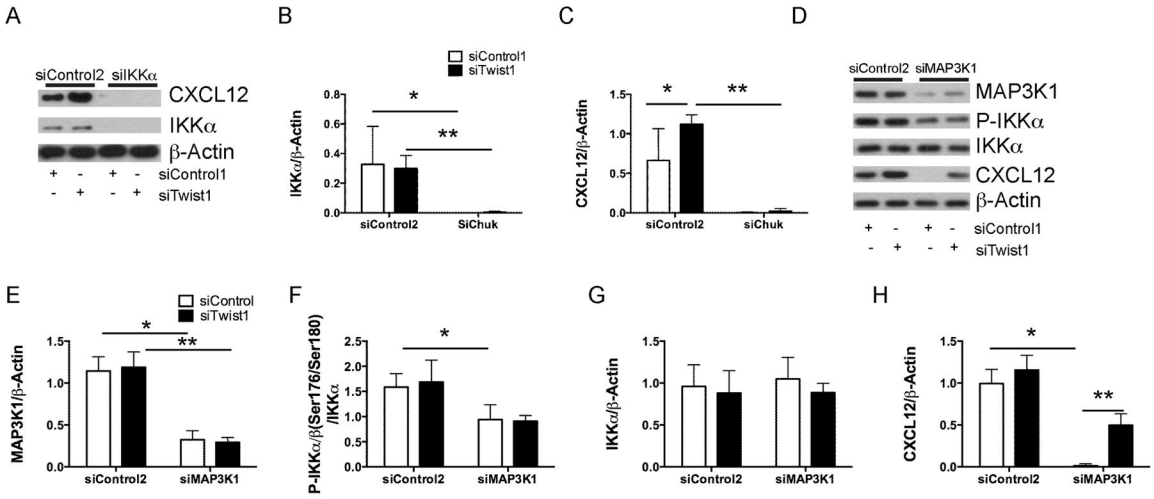

Figure 5. Twist1-mediated regulation of CXCL12 expression is downstream of IKKα

(A) Immunoblotting (IB) of CXCL12 and IKKα from IPF fibroblasts incubated with siTwist1, siIKKα, or both. Data were analyzed by two-way ANOVA followed by Neuman-Keuls post-hoc testing unless otherwise indicated. (B) Band densitometry for IKKα (Chuk) (*P<0.017, siControl1+siControl2 vs siControl1+siIKKα and **P<0.03, siTwist1+siControl2 v siTwist1+siIKKα, N=3) and (C) CXCL12 (*P<0.029, siControl1+siControl2 vs siTwist1+siControl2 and **P=0.0002, siTwist1+siControl2 v siTwist1+ siIKKα, N=3. (D) IB for MAP3K1, phospho-IKKα, total IKKα, and CXCL12 following silencing of twist1, MAP3K1, or both. (E–H) Band densitometry was performed for (D). (E) MAP3K1 (*P<0.0001, siControl1+siControl2 v siControl1+siMAP3K1, **P<0.0001, siTwist1+siControl2 v siTwist1+siMAP3K1, N=3). (F) Phospho-IKKα/β (*P<0.031, siControl1+siControl2 vs siControl1+siMAP3K1, N=3). (G) Total IKKα. (H) CXCL12 (*P<0.0001, siControl1+siControl2 v siControl1+siMAP3K1, **P=0.003, siControl1+siMAP3K1 v siTwist1+siMAP3K1).

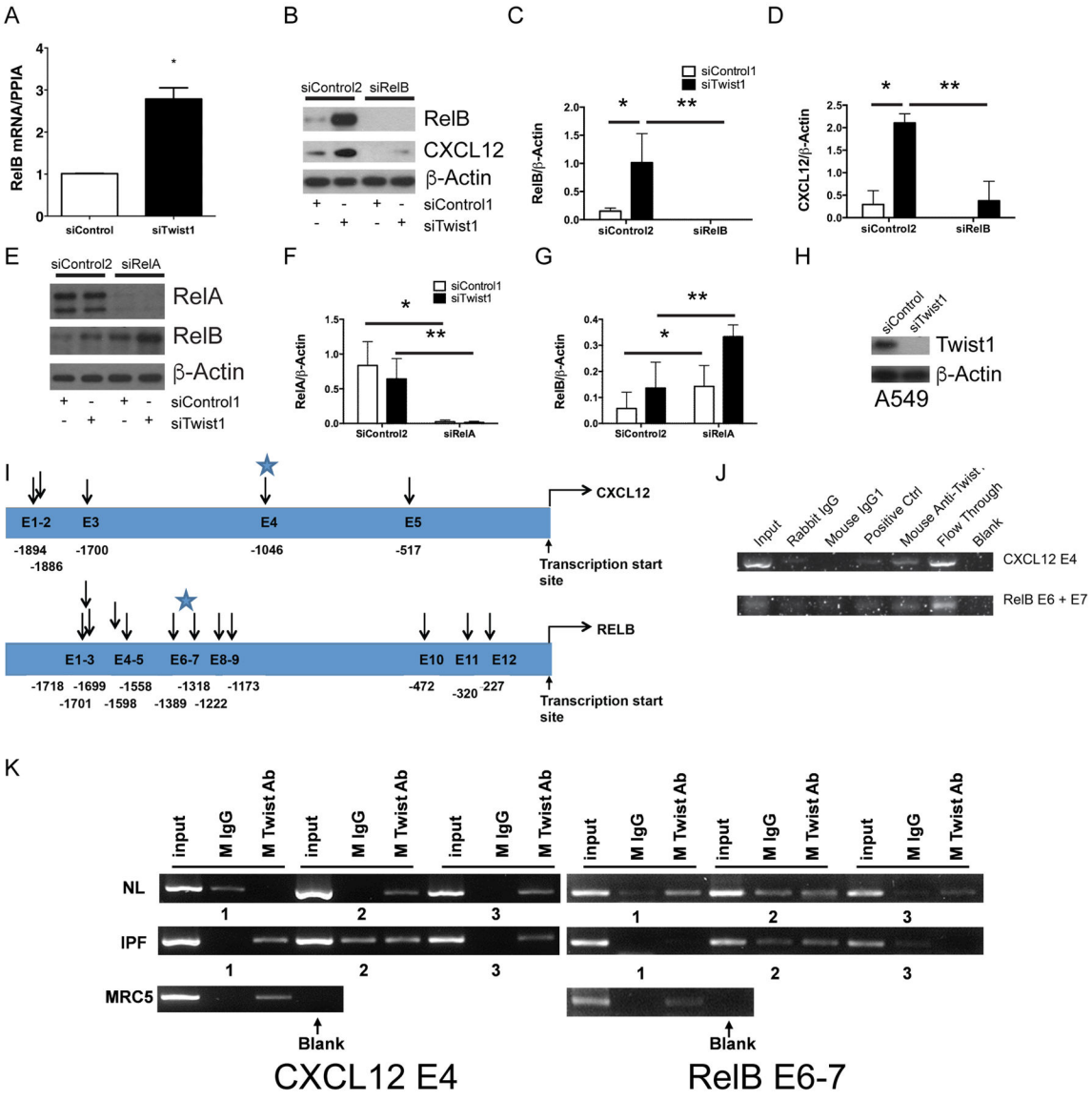

Figure 6. Loss of twist1 in human lung fibroblasts leads to increased expression of RelB

(A) IPF fibroblasts were incubated with siTwist1 or siControl. Cells were processed for quantitative RT-PCR for the non-canonical NF-κB transcription factor RelB (*P<0.003, N=3, by t-test). (B) Immunoblot of IPF fibroblasts following silencing of twist1, RelB, or both. Data were analyzed by two-way ANOVA followed by Neuman-Keuls post-hoc testing. (C) ImageJ quantification of RelB (*P<0.004, siTwist1+siControl2 v siControl1+siControl2 and **P=0.0014, siTwist1+siControl2 v siTwist1+ siRelB, N=3) and (D) CXCL12 (*P<0.0001, siTwist1+siControl2 v siControl1+siControl2 and **P<0.0001, siTwist1+siControl2 v siTwist1+ siRelB, N=3). (E) Immunoblot of IPF fibroblasts following silencing of twist1, the RelB regulator, RelA, or both. (F) ImageJ quantification of RelA (*P=0.002, siRelA+siControl2 v siControl1+siControl2 and **P<0.01, siTwist1+siControl2 v siTwist1+ siRelA, by two-way ANOVA, N=3) and (G) RelB (*P<0.002, siControl1+siRelA v siControl1+siControl2 and **P=0.01, siTwist1+siControl2 v siTwist1+

siRelA, by two-way ANOVA, N=3 (H) Immunoblot of A549 cells with siTwist1 or siControl. (I) Locations of potential E-box motifs identified in the CXCL12 (*top*) and RelB (*bottom*) gene. The starting nucleotide position relative to the transcription start site was listed for each of the potential E-box motifs identified in the upstream sequences of each gene. (J–K) PCR amplification of CXCL12 and RelB upstream sequences using ChIP products from (J) A549 cells and (K) normal, IPF, and MRC5 fibroblasts. For normal and IPF lung fibroblasts, N=3. ChIP assay of the CXCL12 and RelB upstream sequences were performed using mouse antibody specific for twist1. Antibody specific for polII DNA polymerase was used as a positive control and IgG1 purified from rabbit and mouse serum, respectively, were used as negative controls.

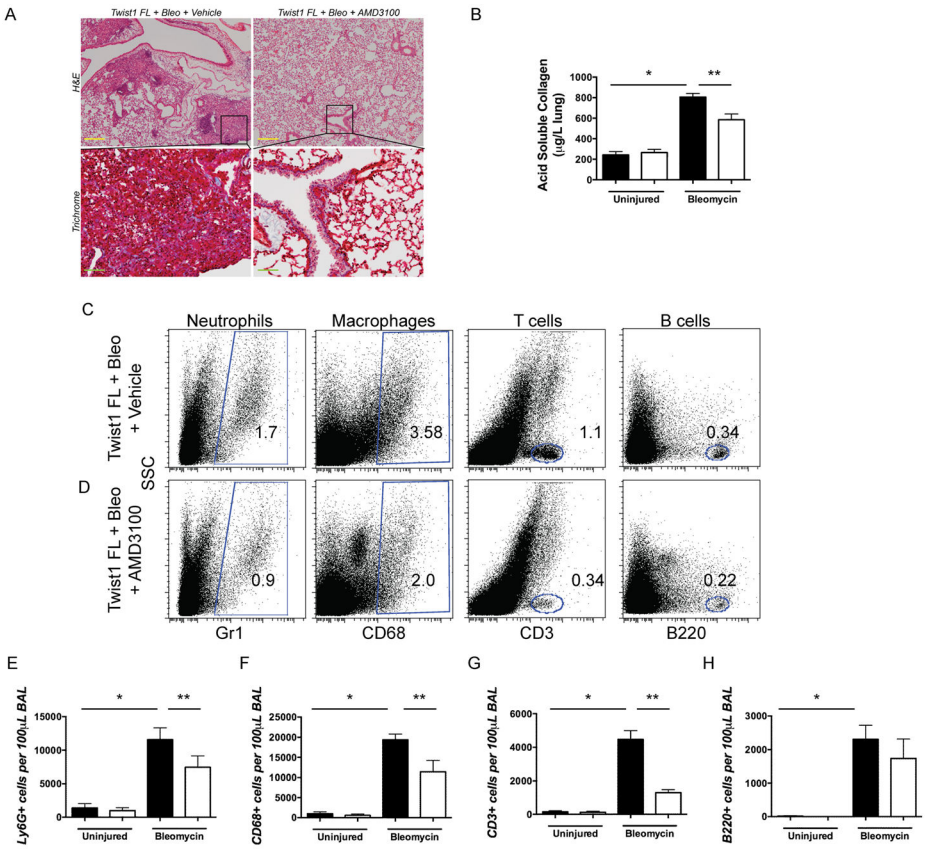

Figure 7. Treatment of bleomycin-injured Twist1 FL animals with the CXCR4 blocker AMD3100 decreased the enhanced pulmonary fibrosis associated with the loss of twist1 and significantly reduced the accumulation of T-cells to the lung

Twist1 FL mice were injured with bleomycin or saline control and then treated with or without the CXCR4 blocker AMD3100. Animals were sacrificed on Day 14. (A) Hematoxylin and Eosin staining and Trichrome staining of lung sections (Inset bar=200μm, magnification ×200). (B) The left lungs were processed for collagen determination by the Sircol Assay (*P<0.0001, Uninjured v Bleomycin, N=8–9 and **P=0.0004 by ANOVA, Bleomycin + vehicle v Bleomycin + AMD3100, N=8–9). Bronchoalveolar lavage was processed for flow cytometry for (C–D) Dot plots for Ly6G+ neutrophils, CD68+ macrophages, CD3+ T-cells, and B220+ B-cells from bleomycin-injured twist1 FL mice treated with or without AMD3100. (E) Ly6G (*P<0.0001, Uninjured + vehicle v Bleomycin + vehicle, N=8–9 and **P<0.04; Bleomycin + vehicle v Bleomycin + AMD3100, N=8–9), (F) CD68 (*P<0.0001, Uninjured + vehicle v Bleomycin + vehicle, N=8–9 and **P<0.002; Bleomycin + vehicle v Bleomycin + AMD3100, N=8–9), (G) CD3 (*P<0.0001, Uninjured + vehicle v Bleomycin + vehicle, N=8–9 and **P<0.0001; Bleomycin + vehicle v Bleomycin + AMD3100, N=8–9), and (H) B220 (*P<0.0001, Uninjured + vehicle v Bleomycin + vehicle, N=8–9). All data were analyzed by ANOVA.

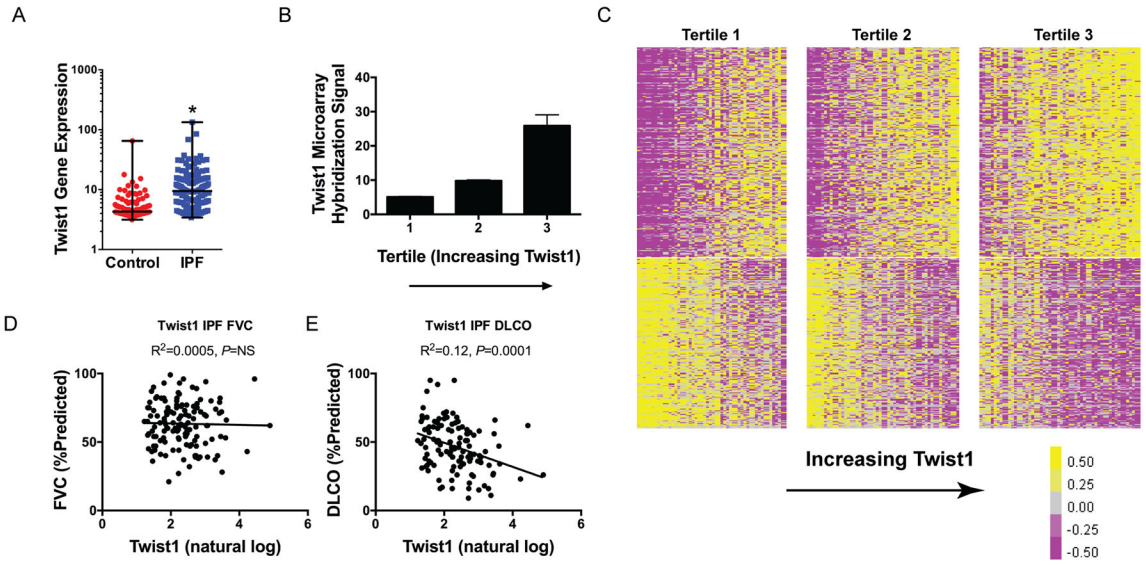

Figure 8. Twist1 gene expression is increased in IPF, and amongst IPF patients, negatively correlates with DLCO in IPF, and is associated with a distinct gene expression profile

(A) Twist1 gene expression was measured in IPF patients (134) and control patients (107). Gene expression was 2.3-fold higher in IPF (*P<0.0001, by unpaired t-test). (B) IPF patients were organized into 3 tertiles based on increasing expression of twist1 (*P*=0.003 for trend by one way ANOVA, n=44–45 per tertile). (C) Heatmap of differentially-expressed genes in IPF patients based on twist1 expression. Each column represents a patient, and each row represents a gene. Between the lowest and the highest tertiles, 387 genes are differentially expressed. (D) FVC (%predicted) and (E) DLCO (%predicted) as a function of natural log transformed twist1 gene expression.

Table 1

Putative E-box Motifs of CXCL12 and RelB Gene

Gene	Location	E-box Motif	Forward Primer	Reverse Primer	PCR Product Size (bp)
RelB	−1718 to −1713	E1	CACATTTGTATATAGCACCCACATG	GAGAAAACTGAAACCCGGCA	123
	−1701 to −1696	E2			
	−1699 to −1694	E3			
	−1598 to −1593	E4	GCCGGGTTTCAGTTTTCTCA	GTGACAGAGTGAGACCTTGTC	128
	−1558 to −1553	E5			
	−1389 to −1384	E6	CCTCGGCCTCCCAAAGTATT	TCTCAGACCACAGATGCAGG	114
	−1318 to −1313	E7			
	−1222 to −1217	E8	TCAGGAATATGAGAGGCTTAGGA	CCTCCGTATACATCCTGAGCT	155
	−1173 to −1168	E9			
	−472 to −467	E10	ATGGATGGCAGGTGTAGAGC	TCTGGACGAGACAACTGAGG	177
	−320 to −315	E11			
	−227 to −222	E12	TGCCCAACCCCTCCTGAG	GACGTCACGCCTGGGGAA	101
CXCL12	−1894 to −1889	E1	CTTTCAGGCTTCTGGGACAG	GTCCGCGGGAAATCTACAC	201
	−1886 to −1881	E2			
	−1700 to −1795	E3	CCTCCCGGGTTTCATCAG	ACTGAAGGCAGTGAGGTCCA	194
	−1046 to −1041	E4	GCTGGGAAGGACACAGAGAG	TGGGTCCAGAAAACTCTTCC	208
	−517 to −512	E5	ACTGCAAAGACGGGTCTCAT	GATGGCGGGAACTGAATG	197

Table 2

LGRC Cohort

	Control	IPF	p-value
N	108	134	
Men (%)	49 (45)	94 (70)	<0.0001
Women (%)	59 (55)	40 (30)	
Age (SD)	63.6 (11.4)	56.4 (11.4)	<0.0001
Ethnicity (%)			
White	100 (92)	122 (91)	0.95
African American	3 (2.8)	5 (3.7)	
Hispanic	1 (0.9)	1 (0.7)	
Asian/Pacific Islander	3 (2.8)	2 (1.4)	
Other	1 (0.9)	1 (0.7)	
Smoking Status (%)			
Never	32 (30)	47 (35)	0.3
Current	2 (1.9)	2 (1.5)	
Ever	63 (58)	81 (60)	
Pulmonary Function			
FEV1, %predicted (SD)	95 (12.6)	70.5 (18.2)	<0.0001
FVC, %predicted (SD)	94.4 (13.1)	63.4 (16.9)	<0.0001
DLCO, %predicted (SD)	84.1 (16.7)	46.7 (19.2)	<0.0001

Table 3

Top 30 Upregulated Genes in the Twist1-low Tertile (Tertile 1)

Gene Symbol	Gene Name	Entrez ID	Fold Change	−log(p-value)
SLC6A4	Solute Carrier Family 6 (Neurotransmitter Transporter), Member 4	6532	4.54	3.68
CA4	Carbonic Anhydrase IV	762	2.99	3.37
HTR3C	5-Hydroxytryptamine (Serotonin) Receptor 3C, Ionotropic	170572	2.94	3.27
CXCL11	Chemokine (C-X-C Motif) Ligand 11	6373	2.78	3.67
SOSTDC1	Sclerostin Domain Containing 1	25928	2.60	3.25
CXCL9	Chemokine (C-X-C Motif) Ligand 9	4283	2.51	4.21
RTKN2	Rhotekin 2	219790	2.50	3.18
FGFBP2	Fibroblast Growth Factor Binding Protein 2	83888	2.37	4.08
GRM8	Glutamate Receptor, Metabotropic 8	2918	2.20	4.12
LRRTM4	Leucine Rich Repeat Transmembrane Neuronal 4	80059	2.04	4.94
KLRF1	Killer Cell Lectin-Like Receptor Subfamily F, Member 1	51348	2.04	4.38
IDO1	Indoleamine 2,3-Dioxygenase 1	3620	2.00	3.29
CD160	CD160 Molecule	11126	1.98	4.24
SH2D1B	SH2 Domain Containing 1B	117157	1.89	3.35
GBP4	Guanylate Binding Protein 4	115361	1.85	6.40
GCOM1	GRINL1A Complex Locus 1	145781	1.84	3.22
CX3CR1	Chemokine (C-X3-C Motif) Receptor 1	1524	1.84	4.33
IZUMO1	Izumo Sperm-Egg Fusion 1	284359	1.83	3.50
COLEC10	Collectin Sub-Family Member 10 (C-Type Lectin)	10584	1.82	3.94
STXBP6	Syntaxin Binding Protein 6 (Amisyn)	29091	1.81	3.25
fam70a	Transmembrane Protein 255A	55026	1.80	4.26
FIGF	C-Fos Induced Growth Factor (Vascular Endothelial Growth Factor D)	2277	1.78	3.11
LRRN3	Leucine Rich Repeat Neuronal 3	54674	1.76	3.95
KCNH6	Potassium Channel, Voltage Gated Eag Related Subfamily H, Member 6	81033	1.74	3.54
CLIC5	Chloride Intracellular Channel 5	53405	1.73	3.77
USHBP1	Usher Syndrome 1C Binding Protein 1	83878	1.72	3.10
SAMD3	Sterile Alpha Motif Domain Containing 3	154075	1.70	4.18
KLRD1	Killer Cell Lectin-Like Receptor Subfamily D, Member 1	3824	1.70	3.12
TNFSF10	Tumor Necrosis Factor (Ligand) Superfamily, Member 10	8743	1.67	>7
P2RY13	Purinergic Receptor P2Y, G-Protein Coupled, 13	53829	1.67	4.22

Table 4

Top 30 Upregulated Genes in the Twist1-high Tertile (Tertile 3)

Gene Symbol	Gene Name	Entrez ID	Fold Change	−log(p-value)
GREM1	Gremlin 1, DAN Family BMP Antagonist	26585	2.86	4.62
PLA2G2A	Phospholipase A2, Group IIA (Platelets, Synovial Fluid)	5320	2.84	3.95
COMP	Cartilage Oligomeric Matrix Protein	1311	2.48	>7
PCSK1	Proprotein Convertase Subtilisin/Kexin Type 1	5122	2.46	3.23
SLN	Sarcolipin	6588	2.43	3.30
c13orf33	Mesenteric Estrogen-Dependent Adipogenesis	84935	2.34	4.94
MMP3	Matrix Metallopeptidase 3	4314	2.32	3.36
ECEL1	Endothelin Converting Enzyme-Like 1	9427	2.31	3.99
RIMS2	Regulating Synaptic Membrane Exocytosis 2	9699	2.27	3.93
SNX31	Sorting Nexin 31	169166	2.26	3.15
BDKRB1	Bradykinin Receptor B1	623	2.26	4.08
SCRG1	Stimulator Of Chondrogenesis 1	11341	2.26	4.44
CHRDL2	Chordin-Like 2	25884	2.26	3.18
SFRP2	Secreted Frizzled-Related Protein 2	6423	2.25	5.47
DIO2	Deiodinase, Iodothyronine, Type II	1734	2.22	6.52
SLC38A11	Solute Carrier Family 38, Member 11	151258	2.19	5.26
MMP11	Matrix Metallopeptidase 11	4320	2.12	4.08
AVPR1A	Arginine Vasopressin Receptor 1A	552	2.07	5.05
CLEC4G	CCR4-NOT Transcription Complex, Subunit 8	339390	2.06	3.50
ASTN1	Astrotactin 1	460	2.06	3.80
GJB2	Gap Junction Protein, Beta 2, 26kDa	2706	2.00	4.03
AGT	Angiotensinogen (Serpin Peptidase Inhibitor, Clade A, Member 8)	183	1.95	5.03
TUBB3	Tubulin, Beta 3 Class III	10381	1.95	4.48
CTHRC1	Collagen Triple Helix Repeat Containing 1	115908	1.94	5.70
IGF1	Insulin-Like Growth Factor 1 (Somatomedin C)	3479	1.93	4.88
FAM55D	Neurexophilin And PC-Esterase Domain Family, Member 4	54827	1.90	3.47
C6orf142	Muscular LMNA-Interacting Protein	90523	1.87	3.78
BDKRB2	Bradykinin Receptor B2	624	1.85	4.51
ATP10B	ATPase, Class V, Type 10B	23120	1.84	3.29
KCTD8	Potassium Channel Tetramerization Domain Containing 8	386617	1.83	3.60

	L23R,ITGAL,KLRC4-KLRK1/KLRK1,LOX,MMP11,MMP3,OAS2,OAS3,PCSK1,PLA2G2A,PRDX2,PSMB9,SCG5,SMAD1,TACR2,TBX21,TIMP1,TLR3,TLR7,TMEM158,TNFAIP6,TNFSF11,TRPC4,WARS
	GFBP6,ITGAL,LOX,MMP3,NGFR,NME1,NPPA,NUMB,OAS2,OAS3,OSMR,PLA2G2A,PPAP2A,PSMB9,RBPMS,SERPINF1,SLC2A4,SMAD1,TBX21,TDRD7,TGFB3,TIMP1,TLR3,TLR7,TNC,TNFAIP6,TNFSF11,TPST1,VIP
	5,IL23R,ITGAL,LGALS1,MMP3,NGFR,NPPA,OAS2,OAS3,OSMR,PLA2G2A,PSMB9,RNF19A,RXRG,SERPINF1,SLC39A14,TBX21,TIMP1,TLR3,TLR7,TNC,TNFAIP6,TNFSF11,TP53BP2,TPBG,VCAN,VIP,WARS
	X21,TGFB3,TIMP1,TLR3,TLR7,TNFAIP6,TNFSF11,VCAN
	KLRK1/KLRK1,KLRD1,KRT10,LOX,LTBP1,MMP11,MMP3,MYO1C,NME1,NPPA,OSR2,PPP2R5A,RBPMS,RHOD,SCG5,SLC39A14,SLN,TBX21,TGFB3,TIMP1,TNC,TNFAIP6,TNFSF11,TUBB3,UCK2,USP25,VCAN,VIP,XPNPEP2
	P,WARS,XPNPEP2
	,PRDX2,PRKCH,PSMB9,PTP4A3,RTKN2,RXRG,SLC2A4,SMOX,TGFB3,TIMP1,TLR3,TNC,TNFAIP6,TNFSF11,TRPC4,TUBB3,UBA7,VIP,YPEL1